

Washington University in St. Louis

Washington University Open Scholarship

McKelvey School of Engineering Theses & Dissertations

McKelvey School of Engineering

Spring 4-30-2019

The Effect of Mechanical Agitator Geometry on Catheter Directed Thrombectomy

Sanghun Alex Lee

Washington University in St. Louis

Follow this and additional works at: https://openscholarship.wustl.edu/eng_etds



Part of the [Engineering Commons](#), and the [Surgical Procedures, Operative Commons](#)

Recommended Citation

Lee, Sanghun Alex, "The Effect of Mechanical Agitator Geometry on Catheter Directed Thrombectomy" (2019). *McKelvey School of Engineering Theses & Dissertations*. 463.

https://openscholarship.wustl.edu/eng_etds/463

This Thesis is brought to you for free and open access by the McKelvey School of Engineering at Washington University Open Scholarship. It has been accepted for inclusion in McKelvey School of Engineering Theses & Dissertations by an authorized administrator of Washington University Open Scholarship. For more information, please contact digital@wumail.wustl.edu.

Washington University in St. Louis
McKelvey School of Engineering
Department of Mechanical Engineering

Thesis Examination Committee:

Guy Genin, Co-Chair

Mohamed Zayed, Co-Chair

Jessica Wagenseil

The Effect of Mechanical Agitator Geometry on Catheter Directed Thrombectomy

By

Sanghun Alex Lee

A thesis presented to the McKelvey School of Engineering of Washington University in
St. Louis in partial fulfillment of the requirements for the degree of Master of Science

May 2019

St. Louis, Missouri

©2019 Sanghun Alex Lee

Acknowledgements

The author would like to thank Dr. Guy Genin and Dr. Mohamed Zayed for their assistance in writing this paper.

Special thanks to the following individuals for their advice and support that were instrumental in the experimentation and writing of this thesis.

- Dr. Kenneth “Tony” Pryse
- John Cashin
- John Garza
- Heather Chung

Special thanks to Dr. Spencer Lake’s biomaterials laboratory for allowing me to borrow the SMD S300 load cell that was tremendously beneficial to this thesis.

Special thanks to the Zayed Lab at Washington University School of Medicine in St. Louis, Department of Surgery, and the distinguished faculty within my department who have reviewed this thesis and helped support the related research.

CONTENTS

I	INTRODUCTION	1
I-A	Device Introduction	1
I-B	Optimization Objectives	3
I-C	Operating Assumptions	3
I-D	Experimental Design Variables	3
I-E	Anticipated Results	5
II	METHODS	6
II-A	Experimental Methodology	6
II-B	Sample Preparation and Rheometer Measurement	6
II-C	Experimental Apparatus Set Up	10
II-D	Full Schematic	11
II-E	Experiment Methodology	12
III	RESULTS AND DISCUSSION	13
III-A	Smoothed Force Graphs	13
III-B	ANOVA Analysis	21
IV	CONCLUSION	22
IV-A	Future Work	23
	References	23
	Appendix A: Rheology Data	24
	Appendix B: Arduino Code	25
	Appendix C: Smoothing Code	26
	Appendix D: Raw Data and ANOVA Analysis for Clot Samples	27
	Appendix E: Complete Raw Data Graphs	32

LIST OF TABLES

I F Values from Analysis of Variance 22

LIST OF FIGURES

1	Table of mechanical lysis devices.	2
2	Left: Front face of the (0,0) geometry. Right: Front face of the (45,70) geometry.	4
3	Right: Side view of the (0,0) geometry. Left: Side view of the (0,70) geometry.	4
4	A chart summarizing the different agitator geometries that were tested. This chart does not include the control geometry of (0,0).	5
5	Non-Shear Angle Cutting versus Shear Angle Cutting	5
6	Squeeze/pull off test step graph of normal force (N) to time (s).	8
7	Left: Graph of expected angular displacement (blue) to actual angular displacement (red). Sample taken at 2.512 rad/s angular frequency. Right: Graph of expected angular displacement (blue) to actual angular displacement (red). Sample is taken at 0.3891 rad/s angular frequency, from frequency sweep step of 0.1-1 rad/s.	9
8	Graph of expected angular displacement (blue) to actual angular displacement (red) during strain sweep step. Taken at an angular frequency of 0.5 rad/s.	10
9	Part A with labels for bolt and instrument placement.	11
10	Part B with labels for bolt and pins.	11
11	Full schematic of experimental setup.	12
12	Sample force to time graph from trial 2 in blood clot for (15,70) geometry.	13
13	Force to displacement graphs of all geometries (α, θ) with a θ value of 20. Three trials per graph.	14
14	Force to displacement graphs of all geometries (α, θ) with a θ value of 45. Three trials per graph.	15
15	Force to displacement graphs of all geometries (α, θ) with a θ value of 70. Three trials per graph.	16
16	Force to displacement graphs of agar trials. α was held at 0, and θ was varied from 0 to 70. Three trials per graph.	17
17	Forward movement peak forces per geometry with α value of 0. Varied by θ . Clot samples on left, agar samples on right.	18
18	Average forward forces after peak penetration per geometry with α value of 0. Varied by θ values. Clot samples on left, agar samples on right.	19
19	Ratio of forces per geometry with α value of 0. Varied by θ values. Clot samples on left, agar samples on right.	19
20	Indentation stiffness per geometry with α value of 0. Varied by θ values. Clot samples on left, agar samples on right.	20
21	Unloading stiffness per geometry with α value of 0. Varied by θ values. Clot samples on left, agar samples on right.	20
22	Rheology data of frequency sweep from 0.1-10 rad/s.	24
23	Rheology data of frequency sweep from 0.1-1 rad/s.	24
24	Rheology data of strain sweep from 0-0.1. Frequency held at 0.5.	24
25	Rheology data of strain sweep from 0-0.1. Frequency held at 1.0.	24
26	Copy of arduino code used to control motor.	25
27	Smoothing matlab code used on clot sample data.	26
28	Smoothing matlab code used on agar sample data.	26
29	Complete data collected for clot samples.	27
30	Complete data collected for agar samples.	27
31	ANOVA analysis used on peak penetration forces. Varied by α and θ	28
32	ANOVA analysis used on forward movement forces. Varied by α and θ	29
33	ANOVA analysis used on change in weight in sample. Varied by α and θ	30
34	ANOVA analysis used on backward movement forces. Varied by α and θ	31

35	Force to time data graphs for clot sample. Taken from VI. 3 trials per row. Top is (0,0), bottom is (0,20).	32
36	Force to time data graphs for clot sample. Taken from VI. 3 trials per row. Top is (0,45), bottom is (0,70).	32
37	Force to time data graphs for clot sample. Taken from VI. 3 trials per row. Top is (15,20), bottom is (15,45).	33
38	Force to time data graphs for clot sample. Taken from VI. 3 trials per row. Top is (15,70), bottom is (30,20).	33
39	Force to time data graphs for clot sample. Taken from VI. 3 trials per row. Top is (30,45), bottom is (30,70).	34
40	Force to time data graphs for clot sample. Taken from VI. 3 trials per row. Top is (45,20), bottom is (45,45).	34
41	Force to time data graphs for clot sample. Taken from VI. 3 trials per row. Row is (45,70). .	34
42	Force to time data graphs for agar sample. Taken from VI. 3 trials per row. Top is (0,0), bottom is (0,20).	35
43	Force to time data graphs for agar sample. Taken from VI. 3 trials per row. Top is (0,45), bottom is (0,70).	35

Abstract

Venous thromboembolism (VTE) is a vascular disease in which a blood clot forms inside of a vein, most often deep in the legs, groin, or arm. Two types of VTE exist, deep vein thrombosis (DVT) and pulmonary embolism (PE). DVT occurs when a clot in a deep vein forms, risking embolism and causing swelling as the clot obstructs blood flow. An embolism occurs when a part or all the thrombus breaks off and travels in the circulation, getting lodged in the lungs. A pulmonary embolism is a very serious medical condition and can be fatal if not treated immediately. Current guidelines for treatment recommend oral administration of blood thinners, but in cases where alternative measures are needed, intervention with catheter directed thrombolysis (CDT) is commonly attempted. Methods for catheter directed thrombolysis vary greatly, but a regular feature is the option for mechanical agitation. The most commonly seen mechanic for mechanical agitation involves an expanding mesh geometry that is expanded either behind or within the thrombus. The issue with mesh geometries lies in the delicate cell lining of the vessel. Any injury to the vessel lining can cause the recurrence of a VTE as a post treatment complication. Mesh geometries risk breakage, and the expanding radial size can risk contact with the vessel lining. To overcome this disadvantage, we present a novel design for mechanical agitation in catheter directed thrombolysis. In this novel method, a rail mounted fin geometry that is constrained to the centerline is advanced and retracted through a sample thrombus to break up the thrombus and restore flow through the vessel. To this end to study this geometry performance, three performance objectives were outlined. The objectives were peak penetration force, average forward movement force, and average mass of sample removed. 3D printed geometries varying in two angles were tested on porcine thrombus samples for the three objectives. Results suggest that the angle of pitch relative to the front face of the geometry, is very impactful on penetration and forward movement.

The Effect of Mechanical Agitator Geometry on Catheter Directed Thrombolysis

By

Sanghun Alex Lee

Master of Science in Mechanical Engineering

Washington University in St. Louis, 2019

Research Advisor: Guy Genin, Mohamed Zayed

Index Terms

Deep Vein Thrombosis, Catheter Directed Thrombolysis, Mechanical Agitator

I. INTRODUCTION

DEEP venous thrombosis and pulmonary embolisms affect as many as 900,000 people in the United States each year, with 60,000-100,000 fatalities being attributed to venous thromboembolism. [1] Among those affected, about one-half will have long term complications known as post-thrombotic syndrome. Numerous factors can increase the risk of VTE in a patient. Injury to a vein can trigger the development of a VTE. Long periods of immobilization can severely increase the risk of a DVT, such as an extended hospital stay or being bedridden. The deep veins in the legs depend on muscle movement to move blood back up the body. Extended time lying down can cause blood to pool in the lower extremities, increasing the likelihood of a clot forming. DVT has been shown to strongly correlate to invasive surgery, any form of decreased blood flow, an increase in estrogen, heart or lung disease, age, or previous history of DVTs. Additionally, nearly 50 percent of all blood clots occur during or immediately following a hospitalization or surgery. As medical technology advances and care becomes more readily available to all, VTE will only become more and more prevalent as a post care concern.

Conservative estimates for the annual cost of treating newly diagnosed VTEs are between \$ 7-10 billion, for 375,000 to 425,000 newly diagnosed, medically treated incident cases. [2] Estimates for the total economic impact of VTE, including the value of lost economic output due to premature mortality, go up to \$69 billion dollars annually. Venous thromboembolism is a widespread problem that will only become more relevant, creating the need for improvements in techniques and devices to treat the disease.




A. Device Introduction

The guideline for treatment of VTE calls for mainly the use of oral pharmaceutical blood thinners. [3] In the cases where the patient's co-morbidities increase the risk when using blood thinners, or they are unable to take the blood thinners due to other concerns, intervention is necessary. [4] Interventional treatment options vary greatly depending on the patients specific needs, from local thrombolytic delivery through catheter directed thrombolysis (CDT) to mechanical agitation. [5] Often, a practitioner will incorporate more than one treatment modality in order to maximise the chances of success. Mechanical agitation as an adjunct to catheter directed thrombolysis can take many forms, from a slightly maneuverable tip, to a curved wire that spins with a high rotation per minute (RPM), to an expanding mesh basket that

Dr. Guy Genin is the Co-Director of the NSF Science and Technology Center for Engineering MechanoBiology and the Harold and Kathleen Faught Professor of Mechanical Engineering in the Departments of Mechanical Engineering and Materials Science Department of Neurological Surgery at Washington University in St. Louis

Dr. Mohamed Zayed is the Director of the Vascular Surgery Biomedical Research Laboratory at Washington University School of Medicine

encapsulates the target. A figure displaying current options for mechanical agitation are shown below in figure 1. As the figure shows, currently available devices for mechanical lysis lack protective measures to ensure that the device has minimal to no contact with the delicate vessel lining. The slightest injury to the vessel lining during mechanical agitation can trigger further VTE formation, rendering any treatment that risks such a thing ineffective.

Name of Device	Overview of Device	Positives	Negatives
 Penumbra Separator	Maneuverable tip is attached to suction port and advanced through patient vasculature while mechanically agitating with tip	Easily maneuvered tip for operator controlled mechanical agitation Simultaneous negative pressure suction can remove loosened emboli	Tip can cause significant damage to vessel periphery Lacking failsafe mechanism to capture any escaped emboli from traveling downstream
 Trellis System	Balloons are inflated on both sides of clot, thrombolytics are locally infused, and curved tube between balloons are spun at high speeds to agitate thrombus	Encapsulates treatment zone to protect from embolization Allows for simultaneous application of thrombolytics along with mechanical agitation	No built-in option for suction, all created emboli and applied pharmaceuticals remained in patient after device removal
 Cleaner Wire	Curved tip is brought locally to thrombus and spun at high speeds to eviscerate clot	Design allows for local application of mechanical agitation Will mechanically agitate whatever is nearby with certainty	Very difficult for practitioner to prevent collateral damage to vessel periphery during agitation Lack of protection from embolization
ClotTrievers/ Vetex/ MegaVac (Image presented below)	Expandable mesh is deployed distally to capture and drag the clot into collection catheter	Good at capturing thrombus and removing it through suction port Distal deployment allows for protection from embolism	Distal mesh does not prevent embolism with certainty, small pieces may travel downstream Mesh may scrape vessel walls to cause damage during retrieval

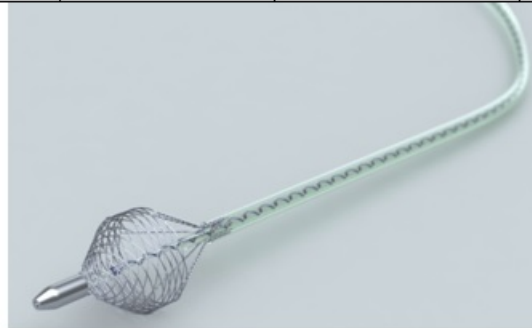


Fig. 1 – Table of mechanical lysis devices.

This thesis is focused on further optimization of a novel method for mechanical agitation; rail mounted, single degree of motion mechanical agitation. In this method, an agitator is pushed over a midline constrained guide rail back and forth through a thrombus to loosen any emboli and to reestablish flow. The key advantage this technique has over competing designs is the ensured safety to the vessel walls. As stated previously, an injury to a vessel wall can trigger the formation or propagation of VTEs. A treatment that removes a large segment of thrombus and restores flow will be pointless if it risks damage to the endothelial cell lining of the vessel wall and triggers future VTE formation. In a rail mounted system, the agitator will always travel along the designated midline path, and if the radius of the agitator

is sufficiently smaller than the radius of the vessel, there is a minimal risk of any contact or damage to the vessel walls.

B. Optimization Objectives

This thesis will focus on the design of the rail mounted agitator fin geometry and testing of different variations, due to a lack of studies on this specific scenario. The objective of this work is to find the agitator geometry design that will travel through a sample clot with the least amount of force necessary, in addition to removing as much of the sample as possible in a single pass. These optimization objectives can be summarized in the following three points.

- 1) Penetration of the thrombus surface by the front face of the agitator with minimal force
- 2) Slicing and cutting by fins during forward movement with minimal force
- 3) Maximal removal of chips/emboli by backward movement with minimal force

C. Operating Assumptions

We operated with several assumptions, to constrain the optimization variables and simplify the problem. In the design of the agitator, only two variables were altered, and all other parameters were unchanged. This list of unchanged parameters includes:

- the central rail size
- the radius of the fins
- the curvature of the fins
- the number of fins
- the spacing of the fins
- the material used in the 3D printing
- the percentage fill of the 3D printing

We will also assume that the negative pressure suction which follows the mechanical agitation step will be powerful enough to remove any and all emboli created during the procedure. The purpose of these assumptions is to limit and to focus the scope of this thesis.

D. Experimental Design Variables

The geometries tested in this experiment are all variations of the same finned design, with two angles being changed, α and θ . α refers to the angle between the fin and the surface of the rod, as labeled below in figure 2. α angle is shown as right angle between fin and rod surface. α is calculated as the tilt from perpendicular plane. When the angle is 90, $\alpha=0$.

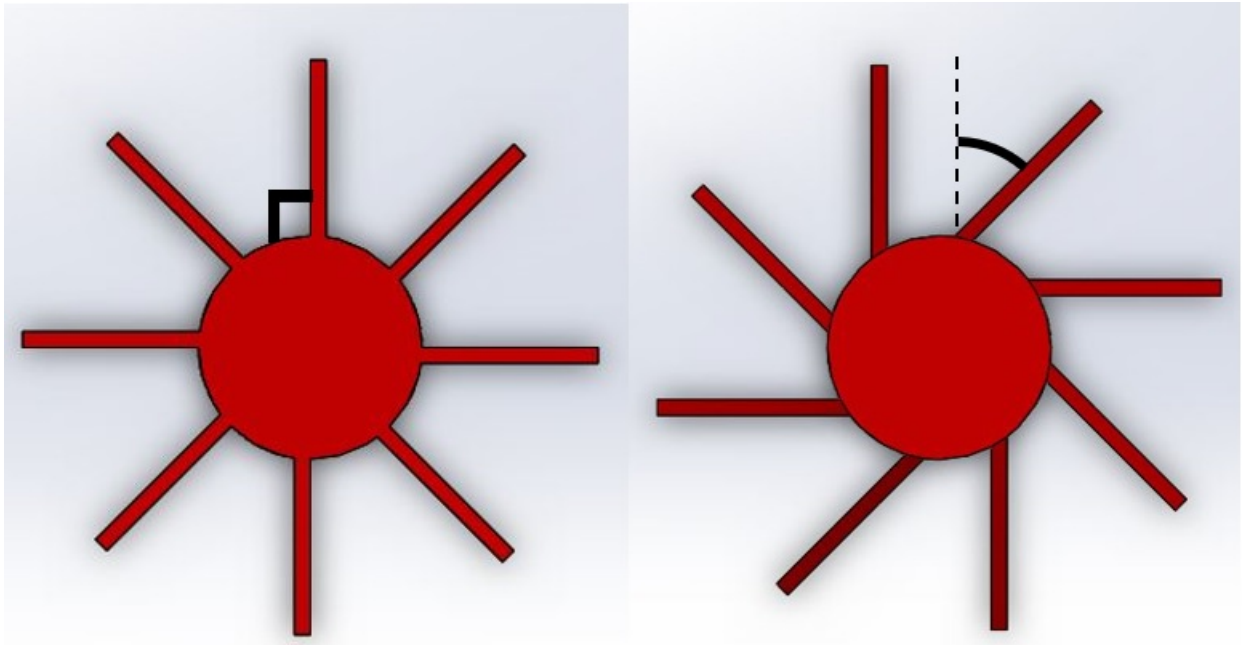


Fig. 2 – Left: Front face of the (0,0) geometry. Right: Front face of the (45,70) geometry.

θ refers to the angle between the front face of the fin and the axis of the rod, as labeled below in figure 3. θ angle is shown as the pitch of the front face, with respect to the front face plane. For a 90-degree angle in the (0,0) geometry, $\theta=0$.

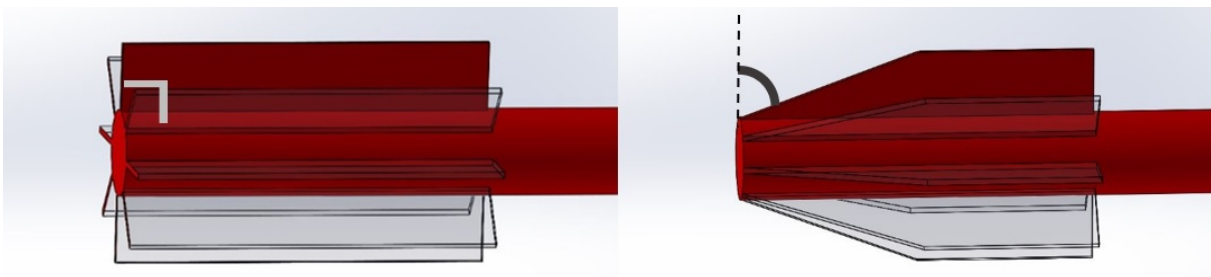


Fig. 3 – Right: Side view of the (0,0) geometry. Left: Side view of the (0,70) geometry.

There were 3 α angle variations used, 20 degrees, 45 degrees, and 70 degrees. There were 4 θ angle variations used, 0 degrees, 15 degrees, 30 degrees, and 45 degrees. Each α variation was applied to each θ variation for a total of 12 geometry variations. Finally, a control geometry of (0,0) was also tested for a total of 13 geometry variations. A chart showing all geometry variations of α and θ is shown below, under figure 4. The chart does not include the control geometry of (0,0).

(α, θ)	20	45	70
0	(0,20)	(0,45)	(0,70)
15	(15,20)	(15,45)	(15,70)
30	(30,20)	(30,45)	(30,70)
45	(45,20)	(45,45)	(45,70)

Fig. 4 – A chart summarizing the different agitator geometries that were tested. This chart does not include the control geometry of (0,0).

E. Anticipated Results

For each of our three optimization objectives, a variable is being altered which we believe will affect each objective.

The first objective was penetration of the thrombus surface by the front face of the geometry. To maximize the pressure applied at a constant force, we thought to minimize the area of front face. This is related to the θ angle, as a steeper slope will create a smaller area in the front face to penetrate the sample. Thus, we hypothesize that geometries with a higher θ value will perform better at this objective. We also hypothesize that α values should have minimal to no impact on penetration of the sample surface as we do not believe it will impact the penetrative force.

The second objective was optimal slicing by the fins of the agitator during forward movement. To minimize the force needed to slice the thrombus as the agitator is pushed forward, we thought to utilize shear angle cutting. Shear angle cutting differs from non-shear angle cutting in that it adds a dimension, going from two-dimensional cutting to three-dimensional cutting. [6] With this method, the same force can be used to exert a higher pressure on the sample to be cut, as the contact area is reduced. A figure illustrating the difference is shown below, under figure 5. We hypothesize that a steeper slope, or a higher θ value, will perform better at forward movement, and that α values will have minimal to no impact on forward movement.

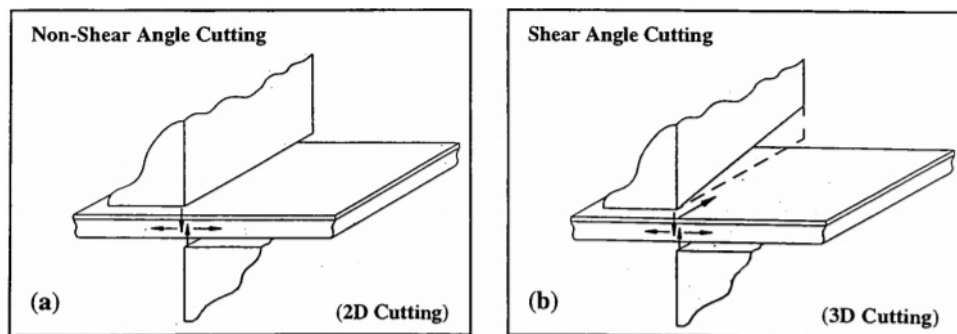


Fig. 5 – Non-Shear Angle Cutting versus Shear Angle Cutting

The final objective was the effective removal of samples with minimal force by backwards movement. To maximize the drag on the chips created during forward movement, curved fins would have been ideal. However, preliminary geometry printing found great difficulty in accurately and reliably printing curved fins. Therefore, the α angle was varied instead of fin curvature. While having a weaker effect than curved fins, we hypothesize that a higher α angle will make the geometry remove more of the sample during backwards movement. We also hypothesize that θ values will have minimal to no impact on this objective.

In Summary: For the first objective of efficient penetration of the sample surface by the geometry front face, we believe that higher θ values will perform better and that α values will have little to no effect.

For the second objective of optimal slicing by fins during forward movement, we believe that a higher θ value will perform better and that α values will have little to no effect. For the third objective of effective removal of samples with minimal force, we believe that a higher α will perform better and that θ will have little to no effect.

II. METHODS

A. *Experimental Methodology*

In this experiment, varying agitator geometry designs were run for a single loop through 20 mL blood clot samples created in Falcon 50 mL conical centrifuge tubes. The agitator geometries were attached to a rail guided linear actuator to ensure consistent movement. The movement was constrained to a vertical single degree of motion, with the blood clot samples being placed underneath the set up. In the connection between the actuator and the agitator geometry, a SMD S300 load cell was placed such that the agitator geometry was hanging from it and any forces, including the weight, acting upon the geometry would be picked up by the load cell. The force readings were then analyzed for the different segments of the motion. Averages were taken for the peak penetration force, the forward motion through the sample, and the backward motion returning to position. The average forces were then normalized with respect to the weight of the geometry. Additionally, the sample was weighed before and after the experiment to get a measure of the mass of the sample that was removed. After analysis of the blood clot samples, additional experiments were run on a non-fibrous agarose material, to provide contrast to the fibrous clot samples. The agar sample experiments were run only on the geometries with an α of 0.

B. *Sample Preparation and Rheometer Measurement*

The mechanical properties of blood clots vary immensely. Variables such as age of the patient, age of the thrombus, location of the thrombus, reason for thrombus formation, and medical history can all drastically change the properties of a thrombus. There are three general classifications for DVT, based on how long the clot has been present. When a clot is 14 days old or younger, it is known as an acute DVT. These types of clots are the softest and the least attached to the vessel walls. This is the type of clot that is the target for this study. Acute clots often pose the highest risk, as the weak attachment to the vessel walls pose a higher threat of breakage, and ultimately, symptomatic pulmonary embolism (PE).

The intermediary stage is known as a subacute DVT, and it contains clots that are between 14-28 days old. At this point, the clot has gotten slightly harder, and the clot has started to form connections to the vessel wall. It is on its way to the final step. In the last classification, chronic DVTs are clots that have been present for over 28 days. Chronic DVTs have hardened and formed connections with the vessel walls, becoming scarred tissue that is very difficult to undo. Chronic DVTs are often associated with a lower risk, as the connections that anchor the hardened thrombus to the vessel will prevent the thrombus from breakage.

The target for this study was acute DVT. For any experimental results to be reliably reproduced, the wide range of possible mechanical properties of blood clots had to be narrowed down and quantified. The values we were interested in were the oscillatory shear modulus, the density, and the age of the clot.

The blood used was food grade porcine blood, obtained from Olive Supermarket. Our lab had been purchasing clotted porcine blood from Olive Supermarket for over a year and have used it as a surrogate to mimic the viscoelastic mechanical properties of an acute stage DVT. In this experiment, we wanted to coagulate the blood inside the centrifuge tubes, rather than slicing out an appropriate sample from a tub as we had been doing. The reasoning was that it would better mimic wall adhesion forces if the clot was able to form inside the tube, as opposed to being placed inside. If the sample were cut out and placed inside, there would be issues with replicability as the geometry of the sample would be difficult to replicate every time and would be inconsistent at best. The adhesion of the sample to the tube would vary drastically and be difficult to measure. By coagulating the blood inside the tube, the sample geometry could be guaranteed to be the same, as the liquid would fill the shape of the container before solidifying.

The supplier sold the blood as dehydrated blood, and the recipe to create the coagulated blood was 60% cold water and 40% dehydrated blood, by volume. No other additives were used. For the 20 mL volume of sample, we used 12 mL of cold water and 8 mL of dehydrated blood. The samples were used in between the 24-48 hour period after the sample was created.

The agar gel sample preparation used 1.5% agar gel by weight. To prepare the agar gel samples, 7.5 g of agar powder was added to 500 mL of boiling water and stirred using a magnetic stirrer until the solution was homogenous. Before the solution was allowed to cool and solidify, a pipet was used to put 20 mL of the solution into the same 50 mL Falcon centrifuge tubes. The samples were then cooled in room temperature and used within 24 hours.

To measure the oscillatory shear modulus, we used a TA AR-G2 rheometer. A 13/16-inch arch punch was used on a sample of blood clot prepared in a petri dish to create disks of sample to be measured. The same size arch punch was used on 150 grain sand paper, and the resulting sandpaper disks were attached to the side of the rheometer head in contact with the sample and the petri dish that the sample was placed on. This aided with surface interaction and worked to prevent slipping. The samples were placed in a 40mm Falcon petri dish on top of the sand paper disks. The petri dish was then inserted into the rheometer.

The rheometer had three programmed steps. The first, a squeeze/pull off test, slowly lowered the rheometer head until the sample exerted a steady normal force of 0.02N (+/- 0.01). This served to set the initial height of the head on top of the sample for the other testing steps. The graph of the normal force with respect to time is given below in figure 6. The characteristic dip in force, caused by surface tension, is then followed by a steady increase until the desired normal force of 0.02N.

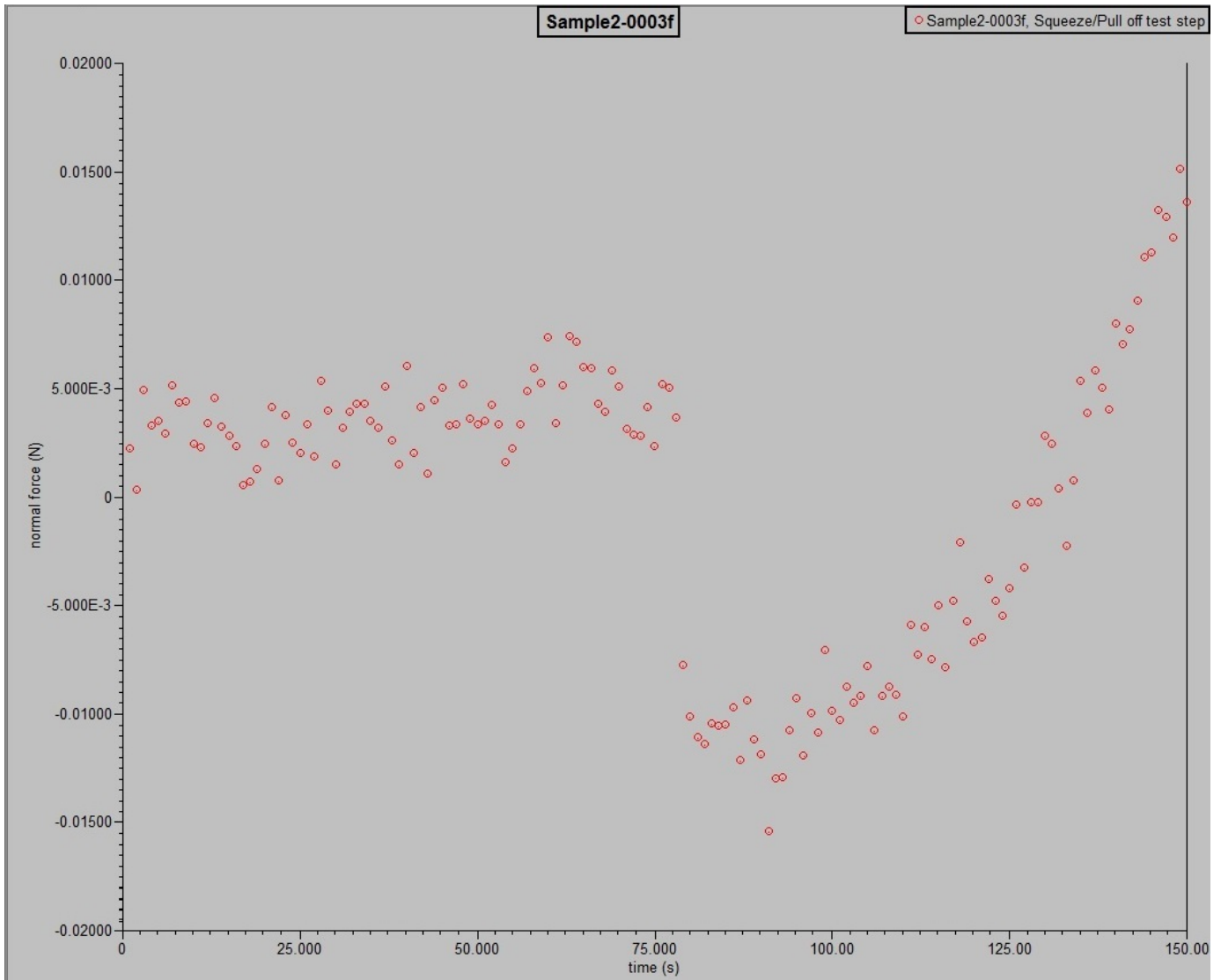


Fig. 6 – Squeeze/pull off test step graph of normal force (N) to time (s).

The next programmed rheometer test step is the frequency sweep step. Initially, the test was performed at a range of angular frequency from 0.1-10 rad/s, with 10 steps taken logarithmically. This yielded some useful data points, but the second half of the test yielded more and more unstable results. The average elastic modulus taken from the usable data point range was 29.97 (+/- 3.82) Pascals. An example of an unstable data point is shown below on the left in figure 7. This data point is unreliable because the expected and actual displacement lines are very different. A usable data point would have the expected and actual displacement lines follow a similar path, as is shown below on the right in figure 7.

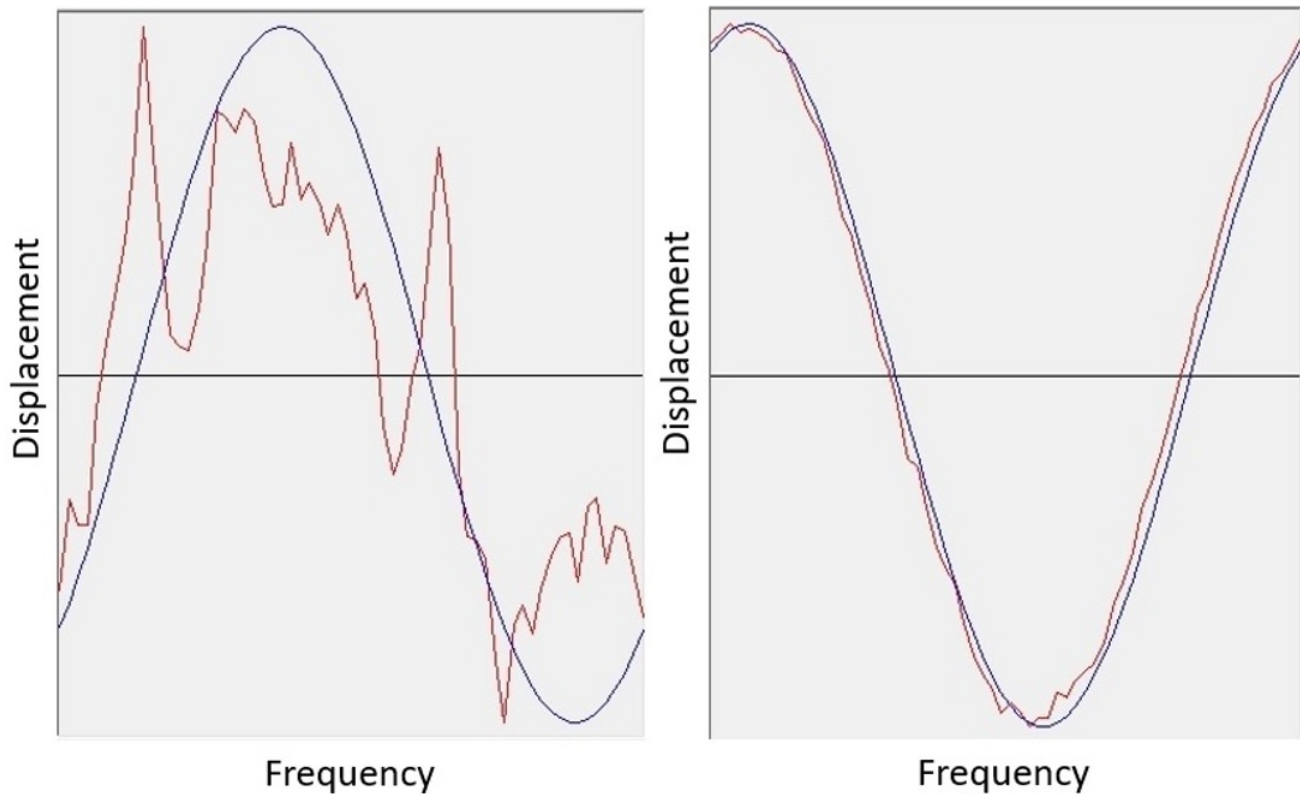


Fig. 7 – Left: Graph of expected angular displacement (blue) to actual angular displacement (red). Sample taken at 2.512 rad/s angular frequency. Right: Graph of expected angular displacement (blue) to actual angular displacement (red). Sample is taken at 0.3891 rad/s angular frequency, from frequency sweep step of 0.1-1 rad/s.

It was determined that the range of angular frequency was too high, and at high angular frequencies the rheometer head was damaging the structural integrity of the sample, rendering any readings past that point unusable. A fresh sample was inserted, with the range of angular frequency changed from 0.1-10 rad/s to 0.1-1 rad/s, with the same number of steps. The adjusted frequency sweep step test that followed yielded reliable data points at every angular frequency increment, for an average elastic modulus of 29.93 (+/- 0.54) Pascals, which was consistent with the first readings. The full set of rheometer data can be found in appendix A.

Finally, the step after the frequency sweep step was the strain sweep step. Where the frequency step varied by angular frequency, strain sweeps held the angular frequency constant and varied the strain. In this case, the strain was varied from 0 to 0.1, at a constant angular frequency of 0.5 rad/s. The angular frequency was decided upon due to reliable readings at around 0.5 in the frequency sweep step. The resulting data gave an average elastic modulus of 26.85 (+/- 1.70738) Pascals. A graph of the expected to actual displacement for a strain of 0.03985 is shown below, in figure 8. The actual displacement closely follows the expected displacement, showcasing a reliable data point.

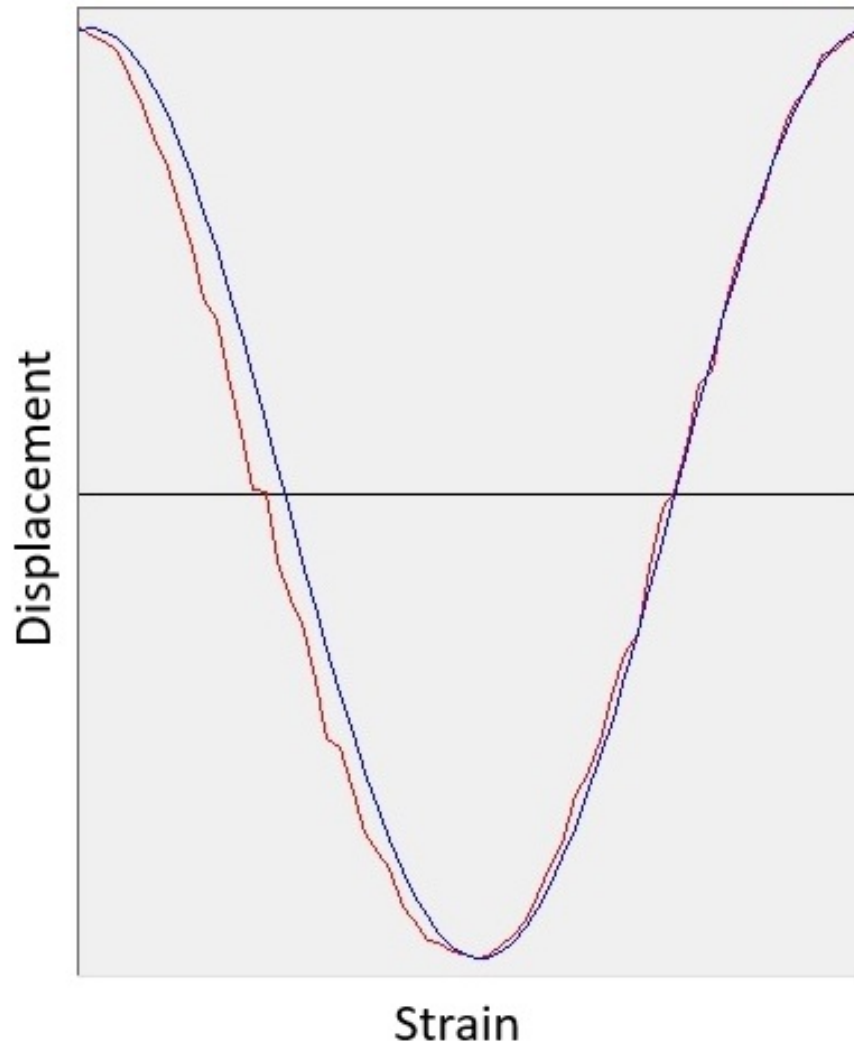


Fig. 8 – Graph of expected angular displacement (blue) to actual angular displacement (red) during strain sweep step. Taken at an angular frequency of 0.5 rad/s.

The density was taken by weighing the sample in the Falcon 50 mL centrifuge tubes and assuming a volume of 20 mL. The average density of all samples was found to be 1.0033 g/mL, which is similar to known values for porcine clots (1.06 \pm 0.01 g/mL). [7] The values should be similar to the density of water, as the majority of the weight is comprised of water.

C. Experimental Apparatus Set Up

The apparatus consisted of two independently controlled sets of instruments that were attached to each other and controlled from the central computer.

The linear actuator set consisted of a 400mm linear stage actuator with a rail guide, powered by a Nema23 24-volt, 3-amp stepper motor. The rail guide was an SFU 1605 level C7 ballscrew. To control the linear actuator, an Arduino was connected to a KNACRO TB6560 stepper motor driver board, which was in turn connected to the Nema23 stepper motor. From the moment the Arduino code was uploaded from the PC, the motor would wait two seconds, move 11.3 cm down, wait one second, and move 11.3 cm up. Then it would rest until the next trial. The Arduino code used is attached in appendix B.

The second set, the force transducer set, utilized a SMD S300 load cell, rated for 2 kg-force. The load cell was connected to an attachment which sent signals to a National Instruments Data Acquisition device (NI DAQ), which was in turn connected to the PC. National Instruments LabView was used to create

and control the virtual instrument (VI). The VI was run simultaneously with the Arduino commands, and recorded force as a function of time.

A connective piece (Part A), was designed and 3D printed to connect the linear actuator stage and the load cell. They were connected to the linear actuator stage by four 6mm hex bolts. The load cell was fastened into place by two 20mm long, 6mm bolts. Part A also connected the sensor attachment, which sent signals to the NI DAQ from the load cell. That was connected on the side by a 4mm hex bolt and nut. Part A is shown below in Figure 9.

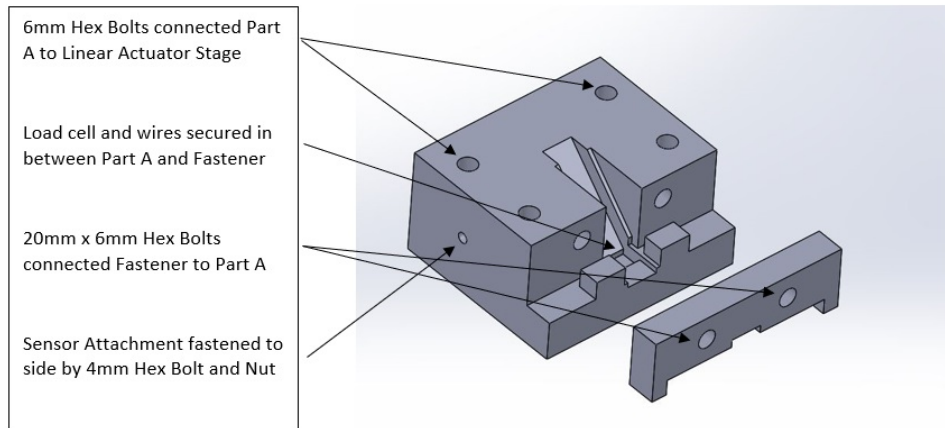


Fig. 9 – Part A with labels for bolt and instrument placement.

Another connective piece, part B, was designed and 3D printed to connect to the load cell and allow for easy geometry replacement. The piece was connected to the load cell by a one inch long, 6-32 screw. The different geometries were connected to part B using a safety pin, for easy exchange. Part B is shown below in Figure 10.

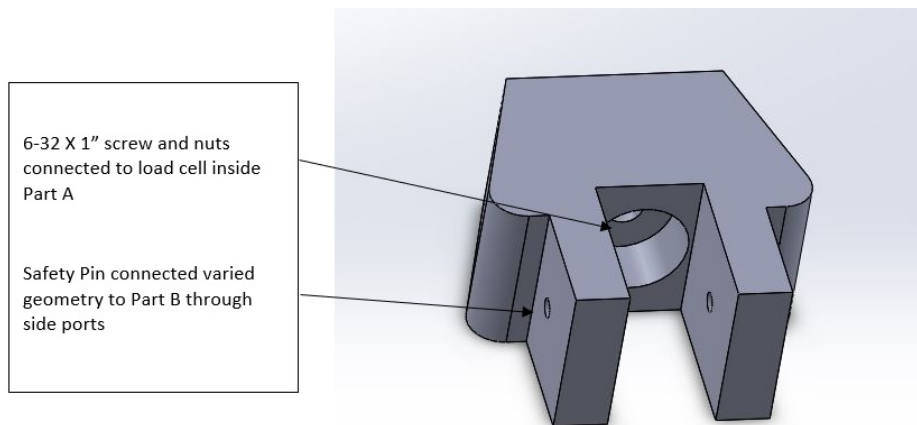


Fig. 10 – Part B with labels for bolt and pins.

D. Full Schematic

The full schematic is shown below with labels for the respective parts, under figure 11.

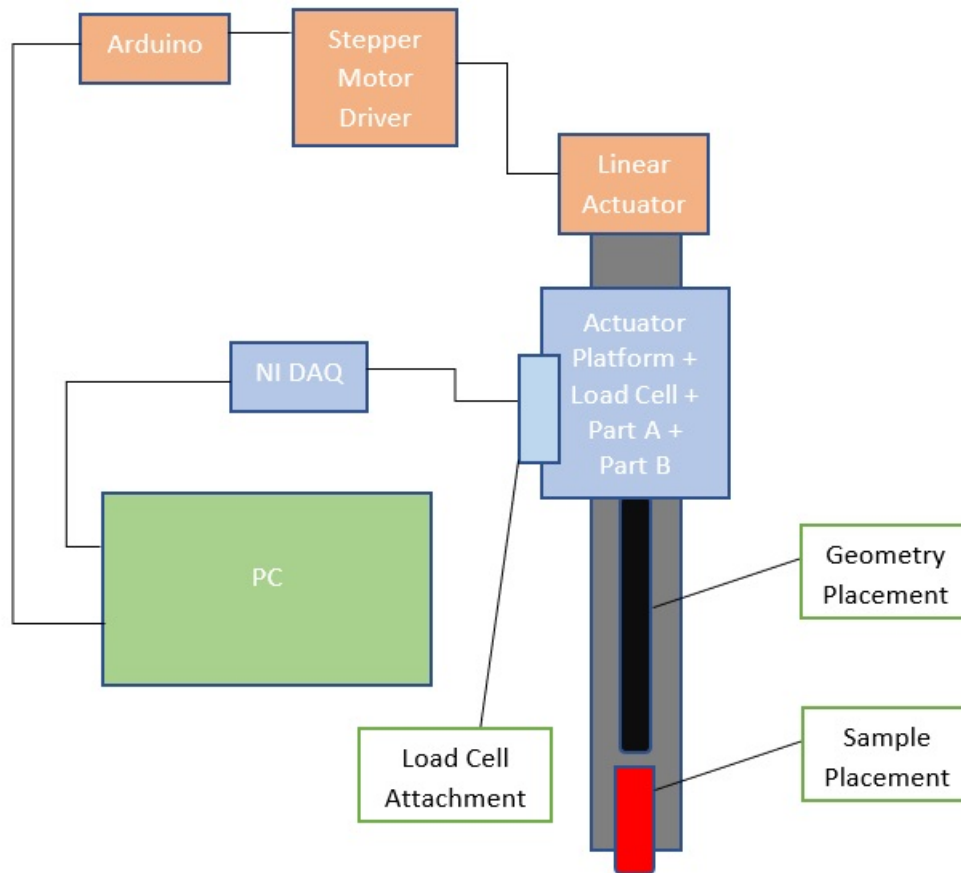


Fig. 11 – Full schematic of experimental setup.

E. Experiment Methodology

The experiment trials began by weighing the sample of thrombus inside the centrifuge tube, without the screw on cap. After recording the before weight, the sample was inserted into the set up and centered axially. The Arduino code was then initialized from the PC. As soon as the Arduino upload was complete, the VI data collection was started. The linear actuator pushed the geometry through the sample and back, while the load cell collected the force data. Once the data collection was finished, the VI was turned off. Then, the geometry was removed, washed with water, dried, and reinserted. Each geometry was tested three times, replacing the clot samples in each trial. If data collection with the geometry was finished, the next geometry was inserted instead. Then the thrombus sample was weighed and the after weight was recorded. The collected data was saved as an image, and the trial data was exported into Microsoft Excel for analysis. The increments of interest with respect to time were recorded for averaging. A pre-motion increment, a peak penetration increment, a forward motion increment, and backwards motion increment were all recorded for each trial, to average. At every instance of the motor starting or stopping, a large spike is seen as the motor initialized. This spike was used as reference in the analysis. An example graph and the increments are shown below in Figure 12.

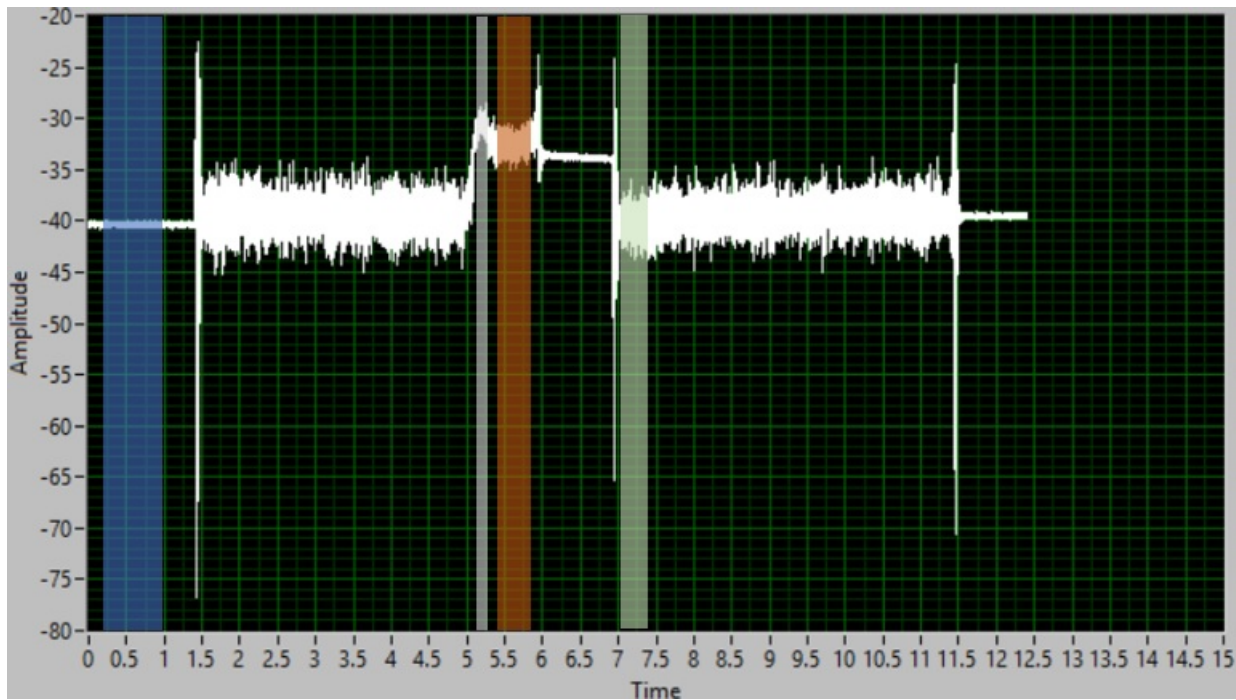


Fig. 12 – Sample force to time graph from trial 2 in blood clot for (15,70) geometry.

From right to left:

- Blue increment shows an example of average weight force. This is before the linear actuator begins movement, and the only force acting on the load cell is the weight of the geometry. This is used to normalize the rest of the readings.
- Grey increment shows an example of peak penetration force. Usually a peak is seen as the geometry tip makes contact with the sample surface, and before it penetrates through the sample surface.
- Red increment shows an example of average forward force. After the peak penetration, there is usually a valley as the penetration finishes, and the sample begins its movement through the sample. The forward force is taken from the valley after the peak penetration until the geometry finishes its movement, which can be seen in the spike in the data.
- Green increment shows an example of average backwards force. After the one second increment after forward movement, the motor begins to move the actuator stage backwards, as evidenced by the plateau followed by a spike. The backwards force is taken from the spike until about 0.5 seconds after, when the geometry leaves the sample.

III. RESULTS AND DISCUSSION

A. Smoothed Force Graphs

The data was smoothed out and zeroed using a Matlab code. The Matlab analysis also converted the time measurements to distance measurements. The result was a distance to force graph of the three trials per geometry design. This visualization of the data allowed for an easier analysis of the trends between the penetration tendencies. The data conversion was done for both the blood clot samples as well as the agar samples. The Matlab code used for the smoothing can be found in appendix C. The raw data graphs can be found in appendix E.

The resulting thrombus sample graphs below highlights the unusual result seen in the θ variance.

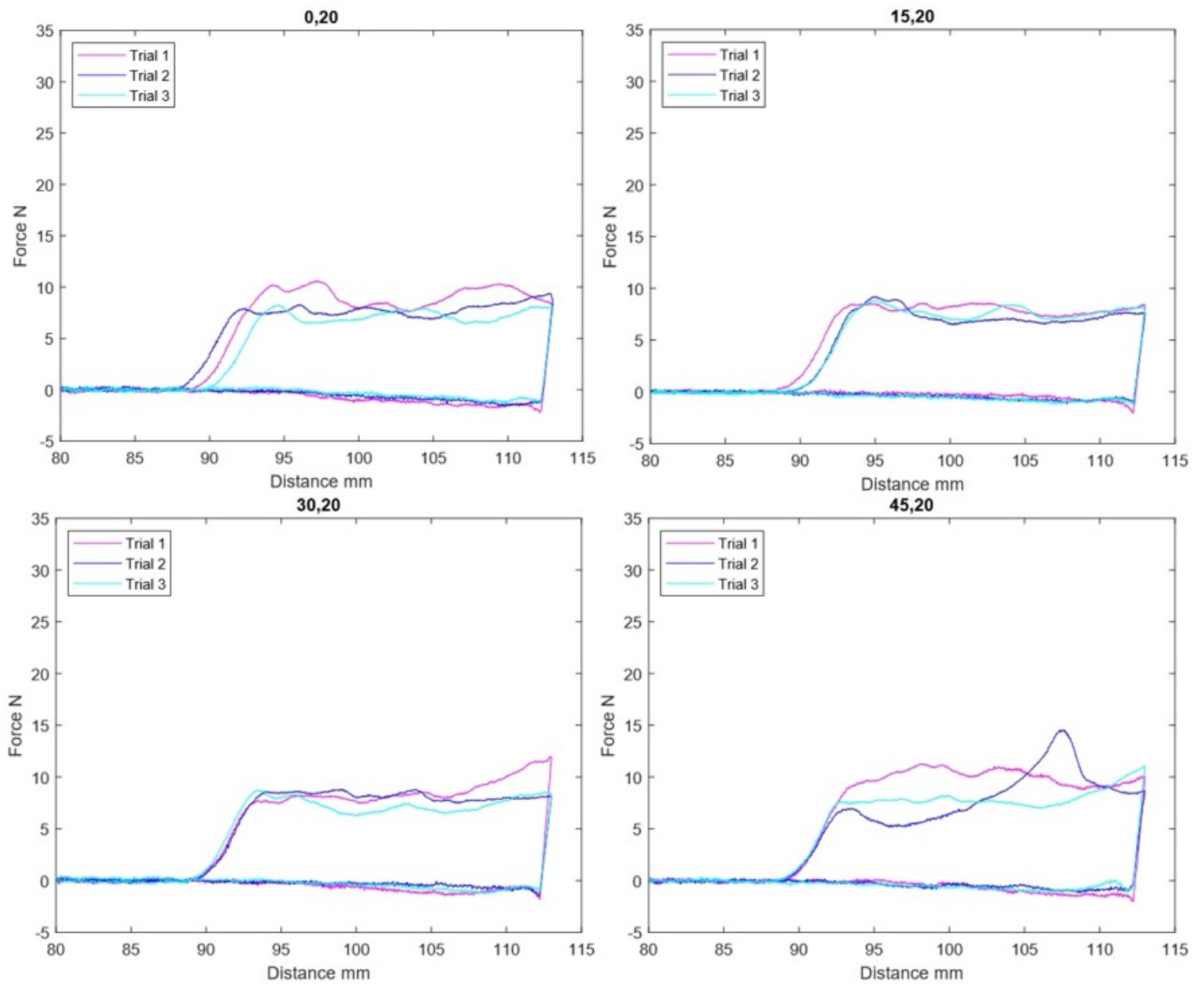


Fig. 13 – Force to displacement graphs of all geometries (α, θ) with a θ value of 20. Three trials per graph.

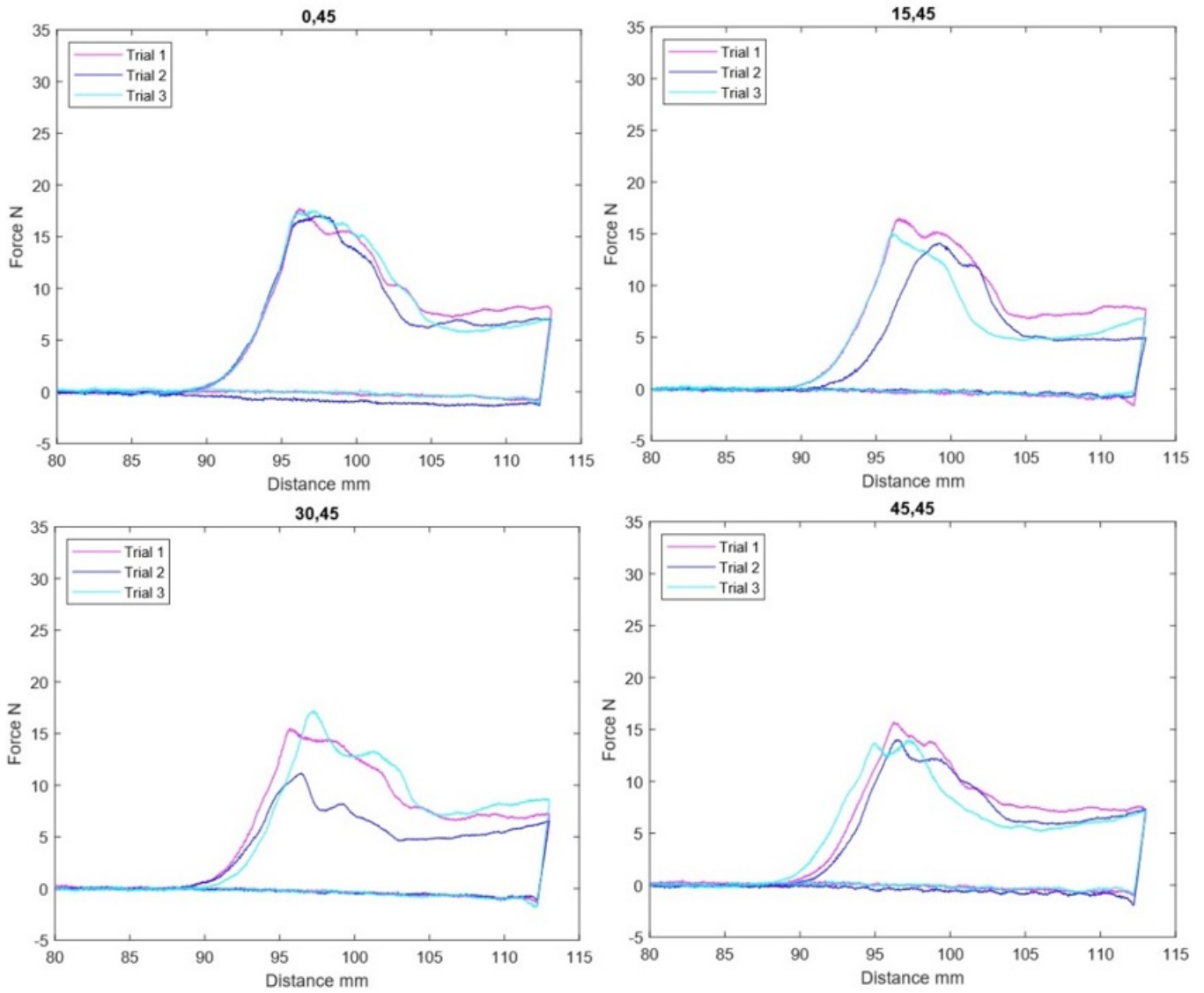


Fig. 14 – Force to displacement graphs of all geometries (α, θ) with a θ value of 45. Three trials per graph.

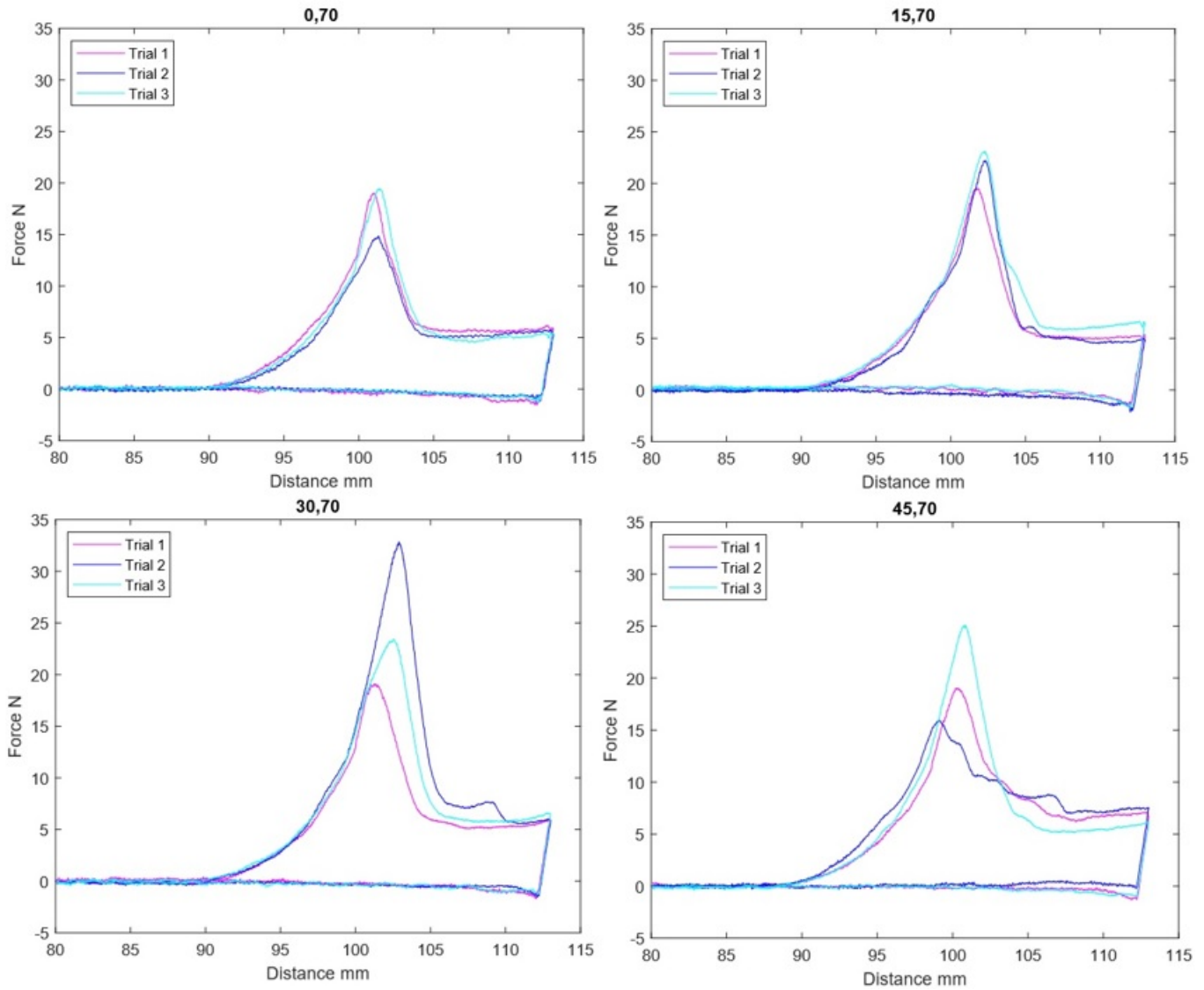


Fig. 15 – Force to displacement graphs of all geometries (α, θ) with a θ value of 70. Three trials per graph.

As the θ increases, one would expect the sharper geometry to require less force to exert the same pressure, as the surface area is decreased. However, the graphs show an increasing trend as the θ is increased, culminating in a spike in the required penetrative force at a θ of 70. This seemingly reversed result can be explained by the fibrin network inside the clot changing the overall stiffness of the sample when the sharp geometry indents and deforms the surface of the sample. Therefore, we would expect the same set of experiments conducted on non-fibrous samples, like the agar samples, to have the opposite trend, where the sharper, high θ values require the least force. The results of the agar trials can be seen below, in figure 16.

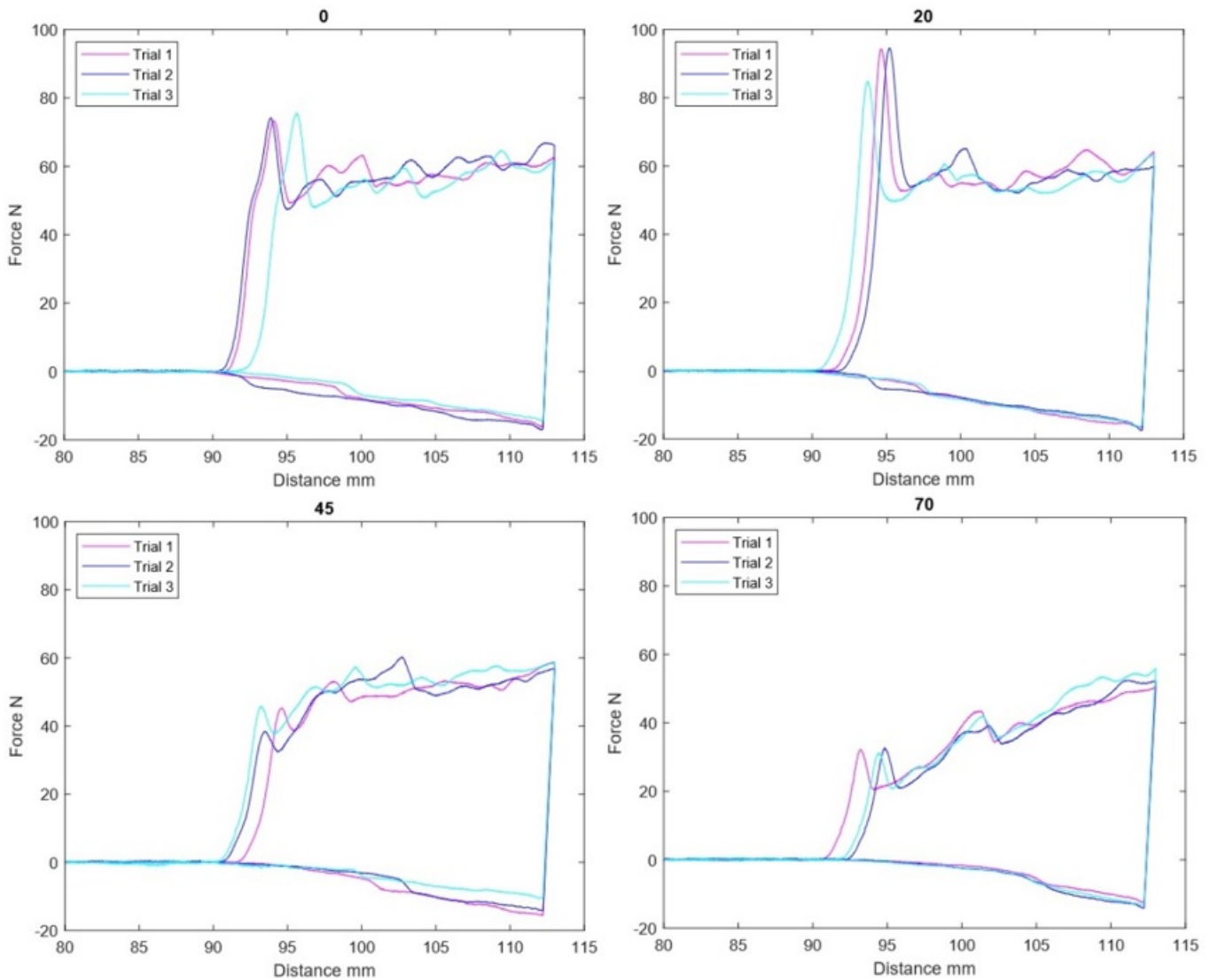


Fig. 16 – Force to displacement graphs of agar trials. α was held at 0, and θ was varied from 0 to 70. Three trials per graph.

As the θ is increased, we see an overall decreasing trend in the penetrative force and forward required force. This is as expected, with the exception to the trend occurring at θ of 20. Here, there is a surprising peak in the penetrative force, an increase from the lower θ value of 0. This results reaffirm the unique mechanical nature of the thrombus samples, and illustrates why designs must account for the fibrous network inside the thrombus and cannot simply assume it to be a non-fibrous material.

There are several geometries with more variance in their trials than other geometries. The most likely explanation for this is inconsistency in the experiment, particularly in the internal structure of the thrombus samples. Notable examples of geometries with large variance in their trials include the (45,20) geometry in figure 14, the (30,45) geometry in figure 15, and the (30,70) geometry in figure 16. The most likely explanation is that there were regions with different distributions of fibrin within the thrombus sample in those trials. In other trials the variance is smaller and not enough to overcome the trends produced by the geometry. However, in trial 2 of the (45,20) geometry in figure 14, there was some irregularity in the fibrin distribution in the thrombus sample that affected the force graph as the geometry pushed through the irregular region of the sample.

In addition to the smoothing graphs, we also extracted the average peak force values per geometry and averaged them. Because of the statistical findings that α was largely unimpactful to the objective performance, we omitted the geometries with α values of 15, 30, and 45, leaving only geometries with

α values of 0. The resulting peak force graphs with standard error bars of both clot and agar samples can be found below, in figure 17.

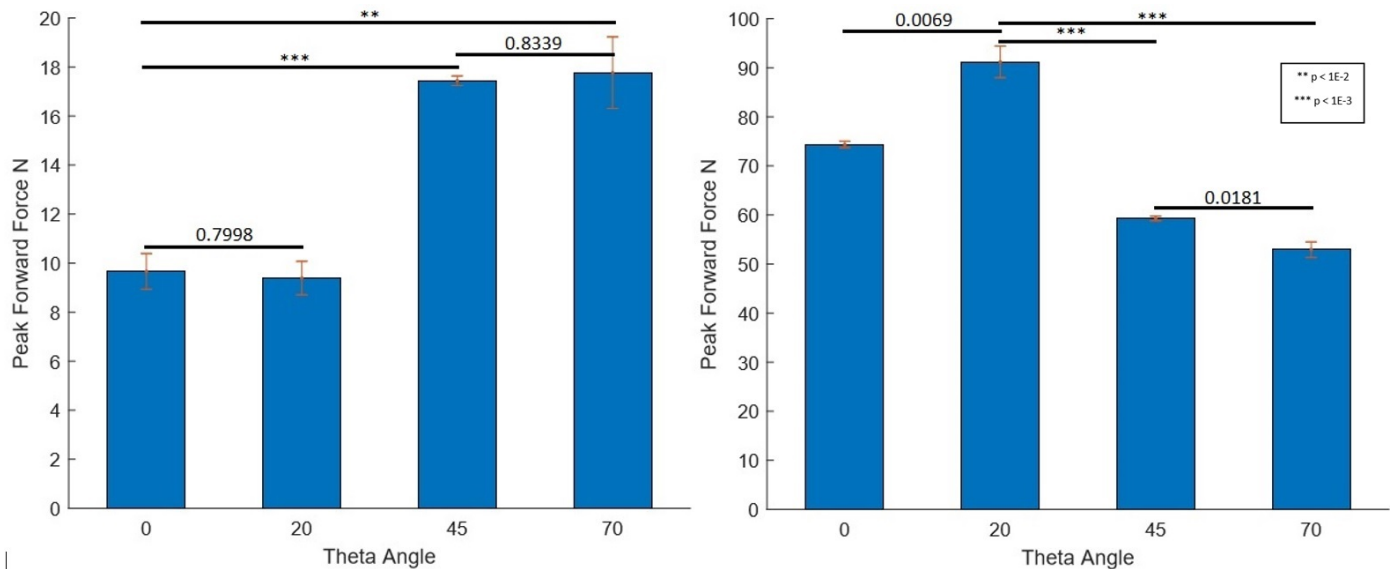


Fig. 17 – Forward movement peak forces per geometry with α value of 0. Varied by θ . Clot samples on left, agar samples on right.

As the trends show in the bar graphs, the trend for the clot samples is the opposite of that seen in the agar samples. The agar samples reflect penetration patterns for a non-fibrous solid, wherein the geometries with a higher θ value and a sharper point, require less force to penetrate. The same surface yield pressure can be achieved with less force because of a smaller area in the sharper geometries. The pattern observed in the clot samples is opposite of this, which reflects the behavior of fibrous solids, wherein the increased surface indentation without yield from the sharper geometries causes the stiffness to increase exponentially, increasing the surface yield pressure. The θ of 20 in agar also departs from the expected pattern. This may be due to a nonlinearity in the sample wherein the higher strain concentrations further increase the stiffness of the agar material. In this case the sharpness of the geometry may have found a middle ground of sorts where the geometry sharply increased the stiffness through the indentation, without providing enough stress to penetrate the material, causing the stiffness to rise higher before penetration occurs.

The average forces and standard error bars during forward movement after penetration, or plateau forces, are shown below in figure 18.

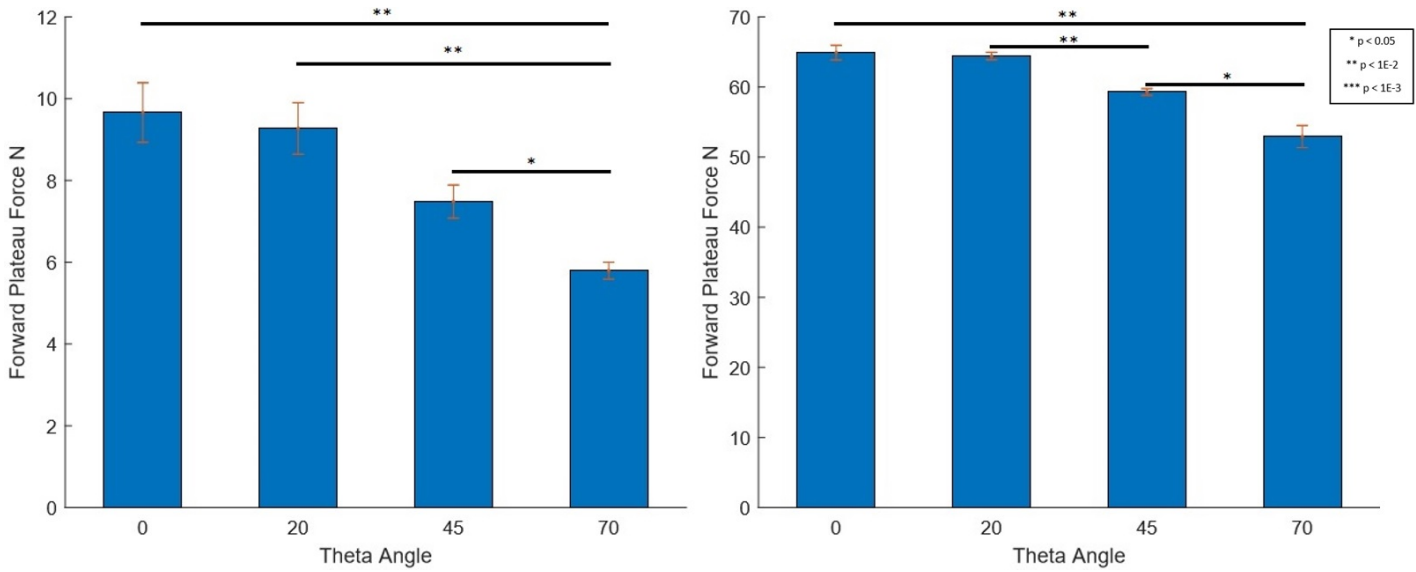


Fig. 18 – Average forward forces after peak penetration per geometry with α value of 0. Varied by θ values. Clot samples on left, agar samples on right.

In both agar and clot samples, the force applied in forward movement was noted to decrease as the θ increased. In both cases, a sharper geometry and a higher θ value perform better at the second objective of cutting during forward movement, after the initial penetration. However, the performance of the geometries on the first objective of initial penetration is a major factor in forces that the vessel wall will feel, as the forces are simply greater for the penetration, which can be seen when comparing the maximum force values for the peak forces versus the plateau forces.

In the next graph, the ratio of peak forces during unloading to the average force during forward movement after penetration for each geometry with an α of 0 is compared. The average of each geometry along with error bars representing the standard error are shown below in figure 19.

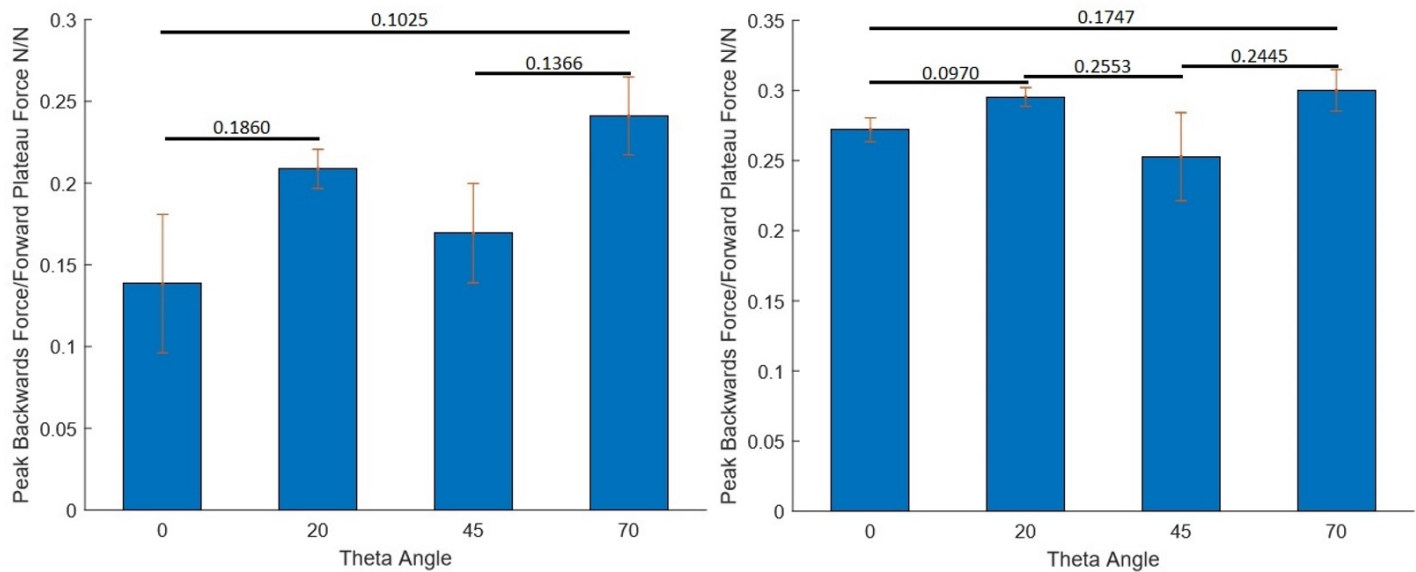


Fig. 19 – Ratio of forces per geometry with α value of 0. Varied by θ values. Clot samples on left, agar samples on right.

The trend in the figure above shows a slight increase in the force applied on the clot samples as the angle of indentation, θ , increases. This further reinforces the finding that forces are reduced by having a lower θ , as the ANOVA analysis showed statistical significance in the variation of θ . In comparison, the

trend in the agar samples is largely horizontal, showing the difference in mechanical behavior between the fibrous thrombin solid samples and the non-fibrous agarose solid samples. The required surface penetration pressure changes as the material is indented without penetration in the clot samples, and does not change in the agar samples. The low variance with respect to the θ angle also suggests that the damaged regions around the insertion had little contribution to the unloading.

The stiffness for the same geometries was also compiled into a bar graph. The stiffness was determined by dividing the change in force by the change in distance during the linear portions of the force by distance graph. The stiffness was calculated for both forward movement, during indentation, and for backward movement, during unloading. The resulting stiffness graphs of both clot and agar samples can be found below, in figure 20 and figure 21. The average per geometry as well as standard error bars are plotted in each graph.

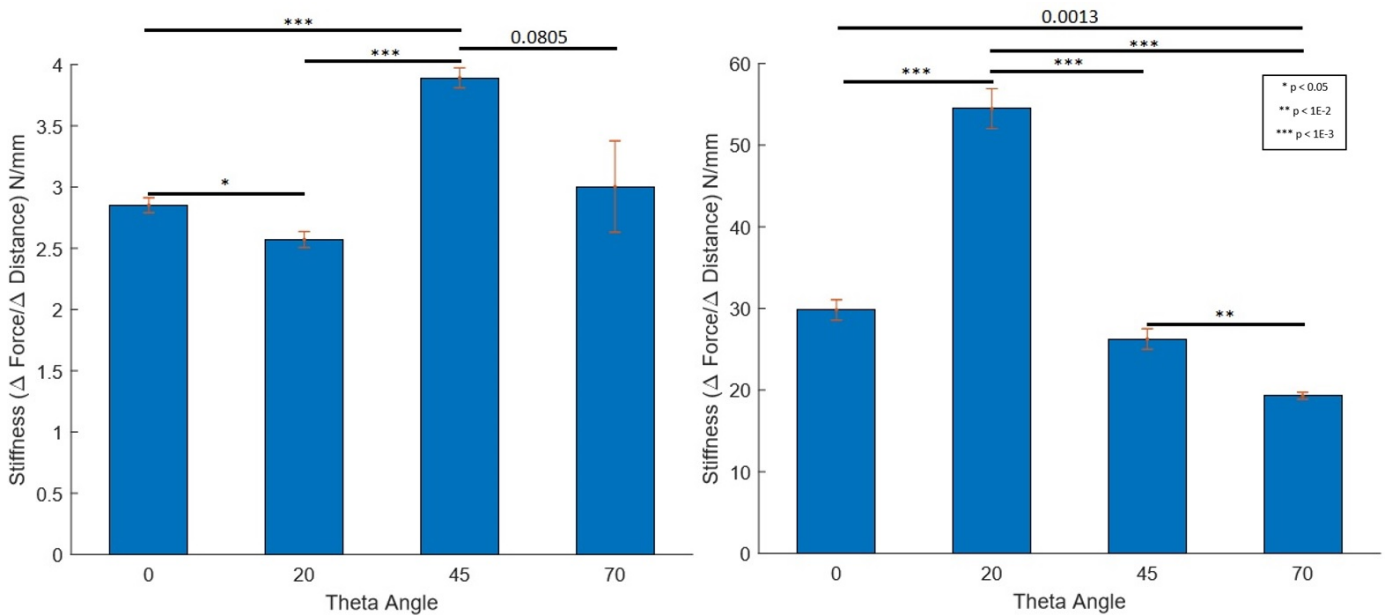


Fig. 20 – Indentation stiffness per geometry with α value of 0. Varied by θ values. Clot samples on left, agar samples on right.

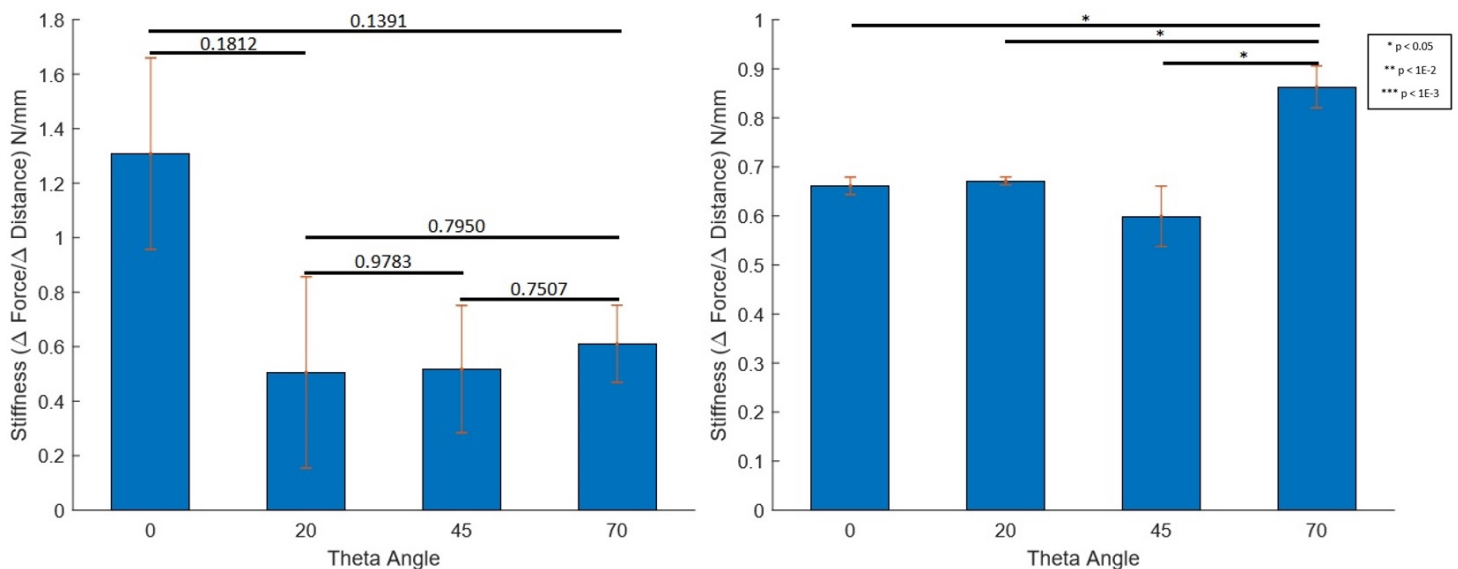


Fig. 21 – Unloading stiffness per geometry with α value of 0. Varied by θ values. Clot samples on left, agar samples on right.

The unloading stiffness for the thrombus samples was found to be higher for a θ of 0, which can be explained by the indentation. In the higher θ values, the fibrous network is indented further before yielding, which would cause further damage to the fibrous network inside the solid. For the θ value of 0, there would have been minimal indentation and therefore minimal damage to the fibrous network, causing the relatively higher unloading stiffness values. In comparison, the unloading stiffness of the other geometries are lower, because of the damage done by the indentation without yield. The unloading stiffness trend for the agar samples are the opposite of the trend for thrombus samples. This supports the indentation damage analysis, as there was no fibrous network to be damaged in the agar samples, and no factor to affect the unloading stiffness values as there was in the thrombus samples.

B. ANOVA Analysis

A two-factor analysis of variance (ANOVA) with replication test was run on all four analyzed increments; the average forward force, the average backwards force, the average peak penetration force, and the average change in weight. In all cases, the null hypothesis was the same. H_1 is that the θ groups have no significant difference in performance. H_2 is that the α groups have no significant difference in performance. H_3 is that the combination of the θ and α groups have no significant difference in performance. This way, by rejecting or failing to reject θ and/or α , we can confirm or deny our initial hypothesis for each of our design objectives. The two factors were the two varied angles, α and θ . The ANOVA was first run for all four with a significance level of 0.05, or 5%. Then the ANOVA was run again with a lower significance level of 0.01, or 1%. Each of the three design objectives are analyzed in detail along with the relevant force set ANOVAs in the following sections. A complete chart of all the data and all ANOVA analysis can be found in appendix D.

The first objective of efficient penetration of the sample surface involves the ANOVA for peak penetration force. At a significance level of 0.05, the critical F value for θ was 3.403 and the critical F value for α was 3.009. The F value for α was 0.535, meaning we fail to reject our null hypothesis that α has no significant change in performance. This is consistent with our hypothesis, where we assumed that α would have little to no effect. The F value for θ was 46.646, meaning we were able to soundly reject the first null hypothesis that θ had no significant impact on performance. This is along the same lines as our hypothesis, but the trend is reversed. We hypothesized that a steeper front face, or a higher θ , would perform better at penetration and need less force. However, the data shows the opposite trend, with a θ of 20 performing far better than a θ of 45 or 70. Finally, the critical F value for the interaction between θ and α was 2.508, and the actual F value was 1.338, meaning we are unable to reject that the combination of θ and α had no significant difference in performance.

The ANOVA test was repeated at a significance level of 0.01. The critical F value for θ changed to 5.614 and the critical F value for α changed to 4.718. The critical F value for the interaction between θ and α changed to 3.667. At this higher significance level, our results were unchanged; the null hypothesis that θ has no significant impact on performance was still soundly rejected and we failed to reject the other two null hypotheses that α has no significant impact and that the combination of α and θ has no significant impact.

Overall, we were able to accurately predict that θ values would have a significant effect on penetration performance, and that α values would have no significant effect on performance. The trend that we observed for θ was surprisingly reversed. With the sharper penetration tip of a high θ , a much higher force was felt, meaning the penetration pressure was far higher than that of a low θ tip. This is likely due to an unforeseen property of fibrous solids, wherein the fibrous fibrin network inside of the thrombus sample exponentially increased the stiffness of the sample when displaced. When the high θ tipped geometries indented the surface of the sample, it displaced the fibrous network and thus a much higher pressure was needed to penetrate the sample.

A table summarizing our findings for this objective is shown below, in Table 1.

The second objective of minimal force during forward slicing involves the ANOVA for average forward force. At both significance levels of 0.05 and 0.01, the critical F values for θ , α , and the combination were

TABLE I – F Values from Analysis of Variance

(F Values)	Penetration	Forward	Weight	Backward	F Critical (0.05)	F Critical (0.01)
θ	46.647	15.525	2.509	2.935	3.403	5.614
α	0.535	2.596	4.223	0.555	3.009	4.718
Combination	1.338	1.583	1.368	2.072	2.508	3.667

unchanged. The F value for α was 2.596, which was close to the critical F value for 0.05 significance, but we failed to reject our null hypothesis that α had little to no effect. When compared to the critical F value for 0.01 significance, we do not reject our null hypothesis with more certainty. This is consistent with our initial hypothesis that α would have little to no impact on the force required for forward movement. The F value for θ was 15.525, meaning we were able to soundly reject the null hypothesis that θ had no significant impact on performance, for both 0.05 and 0.01 significance. This matches our hypothesis that θ would affect the performance of the geometry during forward movement, and the trend is also as expected. The high θ value of 70 outperformed the lower θ values, following the expectations laid out in the hypothesis. The critical F value for the interaction between θ and α was 1.583, meaning we are unable to reject that the combination of θ and α had no significant difference in forward movement performance. This was noted for both levels of significance that were tested.

The third objective of maximal chip/emboli removal during backwards motion involves the ANOVA for average backwards force and the ANOVA for the change in weight in the sample. Again, at both significance levels, the critical F values remained unchanged. The backwards force ANOVA resulted in F values for all parameters that were below the critical F value for 0.05 significance level, meaning we failed to reject our null hypothesis that either variable or the combination of both had little to no effect on backwards force. Indicating that the variations in tested designs had no statistically significant effect on backwards force, and future testing will have to introduce another variable that will have an effect on backwards force.

The ANOVA for weight lost had the F value for α at 4.223, which was higher than the critical F value for a significance of 0.05, but when held under higher scrutiny at a significance level of 0.01, it was found to be lower than the critical F value. So, while we are tempted to reject our null hypothesis that α had no effect on the amount of sample removed in a single trial, we are unable to do so with 99% confidence. It is likely that α has some effect on the mass removed by a geometry, but it is also possible that there are other factors that affect the mass removal, such as surface roughness of the sample or the samples microstructure and composition. This result somewhat confirms the hypothesis that α will impact the weight removal, but also raises questions as to what other variables will aid in the weight removal aspect of a geometry. This will be further discussed in the future plans section. The F value for θ was 2.509, which is less than the critical F values for both significance levels, thus we fail to reject the null hypothesis that θ had little to not effect on weight removal. This is in line with the initial hypothesis.

Our results indicated that the θ angle was very impactful to penetration performance as well as the forward movement performance. However, the trend was the reverse of what was expected. This may be due to the mechanical properties of a fibrous solid, wherein the fibrous network inside the solid exponentially increases the stiffness of the material as it is deformed. This result prompted a second set of experimentation, with a non-fibrous sample being tested instead of the fibrous thrombus sample. As we knew the α angle had little to no effect on any performance objective, we only varied the θ angle and kept the α angle constant at 0.

IV. CONCLUSION

In this experiment, we printed 13 agitator geometries that were varied in two angles, the α angle and the θ angle. We then ran each geometry for three trials through a 20 mL thrombus sample inside of a 50 mL Falcon centrifuge tube, while recording the forces felt by the geometries and the changes in weight of the samples. The data set was then analyzed by running a two way ANOVA to analyze the impact

that both variables, α and θ , had. With the ANOVA tests, we were able to confirm the importance of a shear cutting angle, or the θ angle, for penetration and forward movement of our agitator geometry. We also established that variations in the α angle had little to no effect on the geometry's performance for penetration and forward movement. Finally, we found that the α angle had some effect on the removal of the sample during backwards movement, but there are likely other factors in play that we were unable to account for. Factors such as the roughness of the surface would affect the surface adhesion of the chips from the sample to the geometry, aiding the geometry in the sample removal. With the resources and level of 3D printing that was utilized in this experiment, it would be very difficult to consistently ensure the same level of surface roughness for every geometry, and even harder to vary the level of surface roughness to desired degrees.

A. Future Work

In the future, we would like to perform this experiment set again, but replacing the α variations with a new angle variant. This angle would affect the curvature of the fins, such that they spiral helically around the center. We believe this will impact the backwards force felt by the geometry as well as the fraction of the sample that is removed more so than the α angle. In this study, we were limited by the 3D printing capabilities causing us to be unable to reliably print samples with varying radial spirals. In the future, a higher quality 3D printer will be utilized to reliably print more intricate geometries. In addition, a higher quality printer may allow for surface roughness to be varied with consistency, allowing experiments into not only geometries but also surface conditions.

REFERENCES

- [1] Center for Disease Control and Prevention "Venous Thromboembolism (Blood Clots)" U.S. Department of Health and Human Services. 2018. Web.
- [2] Grosse, S. D., Nelson, R. E., Nyarko, K. A., Richardson, L. C., Raskob, G. E. "The Economic Burden of Incident Venous Thromboembolism in the United States: A Review of Estimated Attributable Healthcare Costs." *Thrombosis Research*. Vol. 137. p. 3-10. 2016.
- [3] Kearon, C., Aki, E. A., Ornelas, J., et al. "Antithrombotic therapy for VTE disease. CHEST Guideline and Expert Panel Report" *Chest*, Vol. 149(2). p. 315-352. 2016.
- [4] Fleck, D., Albadawi, H., Shamoun, F., Knuttinen, G., Naidu, S., Oklu, R., "Catheter-directed thrombolysis of deep vein thrombosis: literature review and practice considerations." *Cardiovascular diagnosis and therapy*. Vol 7(Suppl 3), p.228-237. doi:10.21037/cdt.2017.09.15. 2017.
- [5] Karande, G. Y., Hedgire, S. S., Sanchez, Y., Baliyan, V., Mishra, V., Ganguli, S., Prabhakar, A. M. "Advanced imaging in acute and chronic deep vein thrombosis." *Cardiovascular diagnosis and therapy*, 6(6), 493–507. doi:10.21037/cdt.2016.12.06. (2016).
- [6] Meissner, S. "Mechanics of a shear cutting process." Thesis. Rochester Institute of Technology. 1997.
- [7] Nahirnyak V.M., Yoon, S.W., Holland, C.K., "Acousto-mechanical and thermal properties of clotted blood." *The Journal of the Acoustical Society of America*, 119(6), 3766-3772. 2006.
- [8] Meyers, M. A., Chawla, K. K. "Mechanical Behavior of Materials." Textbook. Cambridge University Press. 2nd Edition. 2008.
- [9] Nguyen, T. N., Babikian, V. K., Romero, J. R., Pikula, A., Kase, C., Jovin, T. G., Norbash, A. M. "Intra-Arterial Treatment Methods in Acute Stroke Therapy." *Frontiers in Neurology*. Vol. 2. 9. 10.3389/fneur.2011.00009. 2011.
- [10] Medgadget. "Covidien's Next-Generation Trellis Peripheral Infusion System for Deep Vein Thrombosis" *Vascular Surgery*. 2014.
- [11] Argon Medical. "CLEANER Rotational Thrombectomy System" Argon Medical Devices. 2018. Web.
- [12] Silver, M. J., Jolly, M., "Acute DVT: Are We Overtreating or Undertreating?" *Endovascular Today*. July 2018. Web.
- [13] Vetex. "Venous Clot Management" Vetex Medical. 2018. Web.
- [14] Medical Expo. "Thrombectomy Catheter/Coronary/Peripheral" Medical Expo. Capture Vascular Systems. 2019. Web.

APPENDIX A RHEOLOGY DATA

ang. frequency rad/s	temperature °C	time s	osc. stress Pa	strain	delta degrees	G' Pa	G'' Pa
0.1	25	126.19	0.3055	9.98E-03	6.396	30.45	3.413
0.1585	25	206.4	0.293	0.010001	5.256	29.27	2.692
0.2512	25	257.35	0.2867	0.010002	3.827	28.84	1.929
0.3981	25	289.9	0.2971	9.98E-03	3.977	30.28	2.105
0.631	25	310.83	0.2894	9.99E-03	4.039	30.37	2.145
1	25	324.36	0.2691	9.99E-03	3.696	30.6	1.977
1.585	25	333.28	0.2201	9.98E-03	3.929	31.33	2.152
2.512	25	339.69	0.09114	9.99E-03	4.144	32.36	2.344
3.981	25	346.84	0.255	9.95E-03	4.455	33.65	2.622
6.31	25	353.86	1.122	1.00E-02	5.389	36.42	3.435
10	25	361.06	3.301	9.96E-03	5.288	41.85	3.874

Fig. 22 – Rheology data of frequency sweep from 0.1-10 rad/s.

ang. frequency rad/s	temperature °C	time s	osc. stress Pa	strain	delta degrees	G' Pa	G'' Pa	ang. frequency rad/s
0.1	25	126.08	0.3104	9.99E-03	10.3	30.61	5.561	0.1
0.1259	25	226.9	0.2936	0.010001	9.398	29.02	4.804	0.1259
0.1585	25	307.21	0.2974	9.99E-03	6.221	29.68	3.235	0.1585
0.1995	25	371.17	0.2923	1.00E-02	5.674	29.23	2.904	0.1995
0.2512	25	422.19	0.2952	9.99E-03	4.932	29.66	2.559	0.2512
0.3162	25	462.95	0.2948	9.99E-03	4.791	29.75	2.494	0.3162
0.3981	25	495.54	0.2936	9.99E-03	4.772	29.84	2.491	0.3981
0.5012	25	521.65	0.292	9.99E-03	4.752	30.01	2.495	0.5012
0.631	25	542.54	0.2891	9.99E-03	4.79	30.26	2.536	0.631
0.7943	25	559.31	0.2829	9.99E-03	4.823	30.46	2.57	0.7943
1	25	572.87	0.2719	9.99E-03	4.988	30.68	2.677	1

Fig. 23 – Rheology data of frequency sweep from 0.1-1 rad/s.

ang. frequency rad/s	temp °C	time s	osc. stress Pa	strain	delta degrees	G' Pa	G'' Pa	ang. Freq rad/s
0.5	25	25.49	0.2866	9.99E-03	4.522	29.5	2.333	0.5
0.5	25	51.605	0.4312	0.015892	4.904	27.93	2.396	0.5
0.5	25	77.75	0.6627	0.025161	5.384	27.12	2.555	0.5
0.5	25	103.88	1.019	0.03985	5.832	26.33	2.69	0.5
0.5	25	130.06	1.551	0.063122	6.837	25.29	3.032	0.5
0.5	25	156.24	2.434	0.10018	7.777	24.95	3.408	0.5

Fig. 24 – Rheology data of strain sweep from 0-0.1. Frequency held at 0.5.

ang. frequ rad/s	temp °C	time s	osc. stress Pa	strain	delta degrees	G' Pa	G'' Pa	ang. Freq rad/s
1	25	12.948	0.2726	9.99E-03	4.677	30.78	2.518	1
1	25	26.551	0.4225	0.015873	4.829	30.09	2.542	1
1	25	40.139	0.6475	0.025156	5.165	29.2	2.64	1
1	25	53.711	0.9798	0.039876	6.095	27.99	2.988	1
1	25	67.33	1.484	0.063004	6.994	26.92	3.303	1
1	25	80.871	2.285	0.099947	8.118	26.16	3.731	1

Fig. 25 – Rheology data of strain sweep from 0-0.1. Frequency held at 1.0.

APPENDIX B ARDUINO CODE

```
// defines pins numbers
const int stepPin = 5;
const int dirPin = 2;
const int enPin = 8;
void setup() {
  // Sets the two pins as Outputs
  pinMode(stepPin,OUTPUT);
  pinMode(dirPin,OUTPUT);
  pinMode(enPin,OUTPUT);
  digitalWrite(enPin,LOW);
}
void loop() {
  //wait a second before starting
  delay(2000);
  digitalWrite(dirPin,LOW);
  // Makes 400 pulses for making two full cycle rotation
  for(int x = 0; x < 4450; x++) {
    digitalWrite(stepPin,HIGH);
    delayMicroseconds(500);
    digitalWrite(stepPin,LOW);
    delayMicroseconds(500);
  }
  delay(1000);
  digitalWrite(dirPin,HIGH);
  // Makes 200 pulses for making one full cycle rotation
  for(int x = 0; x <4450; x++) {
    digitalWrite(stepPin,HIGH);
    delayMicroseconds(500);
    digitalWrite(stepPin,LOW);
    delayMicroseconds(500);
  }
  while(true){
  }
}
```

Fig. 26 – Copy of arduino code used to control motor.

APPENDIX C SMOOTHING CODE

```

close all, clear all
%this is where the excel file is called
[-,sheet_name]=xlsinfo('GroupedClotForces.xlsx');
for k=1: numel(sheet_name)
    data(k)=xlsread('GroupedClotForces.xlsx',sheet_name(k));
    %turns the table into an array
    arrayholder = data(1,k);
    tableholder = table2array(arrayholder);
    titleholder = sheet_name(1,k);
    titleholder_2 = char(titleholder);

    %this is the smoothing function
    %this is the smoothing window variable
    windowSize = 50;
    b = (1/windowSize)*ones(1,windowSize);
    a = 1;
    %it is calling the third column of the array
    thefonzT1 = filter(b,a,tableholder(:,3));
    thefonzT1avg = thefonzT1(319:5062);
    thefonzT1used = thefonzT1(5065:9232);
    thefonzT1Average = mean(thefonzT1avg);
    thefonzT1true = thefonzT1used - thefonzT1Average;
    thefonzT2 = filter(b,a,tableholder(:,4));
    thefonzT2avg = thefonzT2(319:5062);
    thefonzT2used = thefonzT2(5065:9232);
    thefonzT2Average = mean(thefonzT2avg);
    thefonzT2true = thefonzT2used - thefonzT2Average;
    thefonzT3 = filter(b,a,tableholder(:,5));
    thefonzT3avg = thefonzT3(319:5062);
    thefonzT3used = thefonzT3(5065:9232);
    thefonzT3Average = mean(thefonzT3avg);
    thefonzT3true = thefonzT3used - thefonzT3Average;

    figure(k);
    plot((tableholder(5065:9232,1)*10),thefonzT1true,'m');
    axis([80 115 -5 35]);
    hold on
    plot((tableholder(5065:9232,1)*10),thefonzT2true,'b');
    plot((tableholder(5065:9232,1)*10),thefonzT3true,'c');
    hold off
    title((titleholder_2));
    xlabel('Distance mm');
    ylabel('Force N');
    legend('Trial 1', 'Trial 2', 'Trial 3', 'Location', 'NW');
    saveas(gcf,titleholder_2,'pdf');
end

```

Fig. 27 – Smoothing matlab code used on clot sample data.

```

close all, clear all
%this is where the excel file is called
[-,sheet_name]=xlsinfo('GroupedAgarForces.xlsx');
for k=1: numel(sheet_name)
    data(k)=xlsread('GroupedAgarForces.xlsx',sheet_name(k));
    %turns the table into an array
    arrayholder = data(1,k);
    tableholder = table2array(arrayholder);
    titleholder = sheet_name(1,k);
    titleholder_2 = char(titleholder);

    %this is the smoothing function
    %this is the smoothing window variable
    windowSize = 50;
    b = (1/windowSize)*ones(1,windowSize);
    a = 1;
    %it is calling the third column of the array
    thefonzT1 = filter(b,a,tableholder(:,3));
    thefonzT1avg = thefonzT1(319:5062);
    thefonzT1used = thefonzT1(5065:9232);
    thefonzT1Average = mean(thefonzT1avg);
    thefonzT1true = thefonzT1used - thefonzT1Average;
    thefonzT2 = filter(b,a,tableholder(:,4));
    thefonzT2avg = thefonzT2(319:5062);
    thefonzT2used = thefonzT2(5065:9232);
    thefonzT2Average = mean(thefonzT2avg);
    thefonzT2true = thefonzT2used - thefonzT2Average;
    thefonzT3 = filter(b,a,tableholder(:,5));
    thefonzT3avg = thefonzT3(319:5062);
    thefonzT3used = thefonzT3(5065:9232);
    thefonzT3Average = mean(thefonzT3avg);
    thefonzT3true = thefonzT3used - thefonzT3Average;

    figure(k);
    plot((tableholder(5065:9232,1)*10),thefonzT1true,'m');
    axis([80 115 -20 100]);
    hold on
    plot((tableholder(5065:9232,1)*10),thefonzT2true,'b');
    plot((tableholder(5065:9232,1)*10),thefonzT3true,'c');
    hold off
    title((titleholder_2));
    xlabel('Distance mm');
    ylabel('Force N');
    legend('Trial 1', 'Trial 2', 'Trial 3', 'Location', 'NW');
    saveas(gcf,titleholder_2,'pdf');
end

```

Fig. 28 – Smoothing matlab code used on agar sample data.

APPENDIX D
RAW DATA AND ANOVA ANALYSIS FOR CLOT SAMPLES

Trial Number	Scaled Forward	Scaled Backward	Penetration Scaled	Weight Loss
(0,70) T 1	5.420742504	-1.002854749	18.34767354	0.12
(0,70) T 2	5.132728325	-0.309964705	14.41161539	0.15
(0,70) T 3	4.113865804	-0.220263409	19.9171291	0.13
(15,70) T1	4.666200029	-0.490955582	19.04391193	0.11
(15,70) T 2	4.869250439	-0.809628448	22.64207142	0.12
(15,70) T 3	6.284462941	0.085837637	23.3048465	0.11
(30,70) T 1	4.857868858	-1.05239218	18.03922389	0.13
(30,70) T 2	6.305980307	-0.643630716	33.07199589	0.24
(30,70) T 3	6.044749807	-0.462042294	23.13825388	0.17
(45,70) T1	7.681811527	0.429043633	19.90022662	0.29
(45,70) T2	8.003159549	-0.086543302	15.89767354	0.31
(45,70) T 3	7.097565308	1.324868178	26.91383513	0.21
(0,45) T 1	9.08444959	0.986644978	18.28476956	0.36
(0,45) T 2	7.792211082	-0.119441828	17.87031871	0.16
(0,45) T 3	6.255817663	-0.324074963	17.26978362	0.22
(15,45) T1	8.891883103	0.691270412	18.1066394	0.25
(15,45) T 2	4.173249072	-0.89363735	13.10312587	0.15
(15,45) T 3	5.387816392	-0.299727038	15.06495505	0.15
(30,45) T 1	6.987565668	-0.461515398	15.04741913	0.25
(30,45) T 2	7.168833022	1.426046291	12.93606282	0.26
(30,45) T 3	8.813278465	0.505064381	17.87735275	0.26
(45,45) T1	6.896255017	-0.791340826	15.10532084	0.22
(45,45) T2	6.980475165	-0.005722872	14.76294991	0.19
(45,45) T 3	5.992637088	-0.430049734	13.17674385	0.22
(0,20) T 1	9.177356858	-1.151602579	10.50527825	0.19
(0,20) T 2	7.3542171	-1.815569439	6.973532808	0.22
(0,20) T 3	7.532430782	-0.643933118	8.003478306	0.15
(15,20) T1	8.137947158	-0.345969373	8.49153201	0.21
(15,20) T 2	8.054458351	0.221562627	9.981986638	0.12
(15,20) T 3	7.832033625	-0.569920817	8.759935614	0.18
(30,20) T 1	9.58296083	-0.730686347	8.367082627	0.39
(30,20) T 2	8.878774436	0.299869899	9.446896424	0.21
(30,20) T 3	6.816035545	-0.948120385	7.880952859	0.17
(45,20) T1	9.880550931	-1.401677951	9.972572411	0.31
(45,20) T2	10.81999648	0.420950002	7.314863196	0.23
(45,20) T 3	8.154928848	-0.685783458	7.636342925	0.2
(0,0) T 1	8.095392715	0.687230113	6.131661077	0.27
(0,0) T 2	7.666321727	-0.787971752	6.723822849	0.24
(0,0) T 3	9.042939327	0.432420124	7.672380356	0.19

Fig. 29 – Complete data collected for clot samples.

Trial number	Average Weight	Average Forward	Average Backward	Peak Pen	Before Weight (g)	After Weight (g)
0,0 T 1	-39.09665841	18.90681749	-49.97117287	39.10071667	30.35	30.07
0,0 T 2	-40.62037238	19.34233226	-49.18048629	39.02663043	30.32	30.31
0,0 T 3	-39.12994241	17.09492545	-44.44894411	23.45000932	29.48	29.19
0, 20 T 1	-39.80337017	18.99370527	-50.83489658	65.27068	30.63	30.51
0, 20 T 2	-39.10548034	18.06045603	-49.27244719	65.81765263	30.19	30.15
0, 20 T 3	-39.93091682	16.37037881	-50.73578768	53.38840526	30.63	30.36
0,45 T 1	-39.51311647	11.9061114	-46.27219132	8.876353636	30.17	29.84
0,45 T 2	-39.80417994	11.63200543	-50.90358941	-1.717609192	30.34	29.63
0,45 T 3	-39.66267027	13.54079849	-45.54289248	6.923999739	30.71	30.27
0,70 T 1	-40.20455199	-0.69566538	-45.46647492	-4.873684677	30.66	30.31
0,70 T 2	-39.95152705	0.386590685	-43.97345992	-3.801025	29.74	29.69
0,70 T 3	-40.16484499	1.919005507	-44.50693974	-6.295059688	29.93	29.79

Fig. 30 – Complete data collected for agar samples.

Alpha 0	Alpha 15	Alpha 30	Alpha 45	ANOVA: Two-Factor With Replication					Alpha 0,01						
18.34767354	19.04391	18.03922	19.90023	SUMMARY	Alpha 0	Alpha 15	Alpha 30	Alpha 45	Total	SUMMARY	Alpha 0	Alpha 15	Alpha 30	Alpha 45	Total
14.4161539	22.64207	33.072	15.89767	Theta 70					Theta 70						
19.9171291	23.30485	23.13825	26.91384	Count	3	3	3	3	12	Count	3	3	3	3	12
18.28476956	18.10664	15.04742	15.10532	Sum	52.67642	64.99083	74.24947	62.71174	254.6285	Sum	52.67642	64.99083	74.24947	62.71174	254.6285
17.87031871	13.10313	12.93606	14.76295	Average	17.55881	21.66361	24.74982	20.90391	21.21904	Average	17.55881	21.66361	24.74982	20.90391	21.21904
17.26978362	15.06496	17.87735	13.17674	Variance	8.044404	5.256931	58.44393	31.09449	25.83287	Variance	8.044404	5.256931	58.44393	31.09449	25.83287
10.50527825	8.491532	8.367083	9.972572	Theta 45					Theta 45						
6.973532808	9.981987	9.446896	7.314863	Count	3	3	3	3	12	Count	3	3	3	3	12
8.003478306	8.759936	7.880953	7.636343	Sum	53.42487	46.27472	45.86083	43.04501	188.6054	Sum	53.42487	46.27472	45.86083	43.04501	188.6054
				Average	17.80829	15.42491	15.28694	14.34834	15.71712	Average	17.80829	15.42491	15.28694	14.34834	15.71712
				Variance	0.260435	6.355961	6.147116	1.058779	4.290507	Variance	0.260435	6.355961	6.147116	1.058779	4.290507
H1	Theta groups have equal mean			Theta 20					Theta 20						
H2	Alpha groups have equal mean			Count	3	3	3	3	12	Count	3	3	3	3	12
H3	Both groups together have equal mean			Sum	25.48229	27.23345	25.69493	24.92378	103.3345	Sum	25.48229	27.23345	25.69493	24.92378	103.3345
				Average	8.494096	9.077818	8.564977	8.307926	8.611205	Average	8.494096	9.077818	8.564977	8.307926	8.611205
				Variance	3.298836	0.631151	0.642417	2.104123	1.302702	Variance	3.298836	0.631151	0.642417	2.104123	1.302702
				Total					Total						
	Count	9	9	9	9	9	9	9	36	Count	9	9	9	9	36
	Sum	131.5836	138.499	145.8052	130.6805					Sum	131.5836	138.499	145.8052	130.6805	
	Average	14.6204	15.38878	16.20058	14.52006					Average	14.6204	15.38878	16.20058	14.52006	
	Variance	24.0241	32.76215	65.89339	38.32947					Variance	24.0241	32.76215	65.89339	38.32947	
	ANOVA			ANOVA					ANOVA						
	Source of Variation			Source of Variation					Source of Variation						
	SS	df	MS	F	P-value	Fcrit				SS	df	MS	F	P-value	Fcrit
	958.8904	2	479.4452	46.64674	5.39E-09	3.402826	Sample			958.8904	2	479.4452	46.64674	5.39E-09	5.613591
	16.50447	3	5.501489	0.535257	0.66257	3.008787	Columns			16.50447	3	5.501489	0.535257	0.66257	4.718051
	82.5053	6	13.75088	1.337867	0.279295	2.508189	Interaction			82.5053	6	13.75088	1.337867	0.279295	3.666717
	246.6771	24	10.27821				Within			246.6771	24	10.27821			
	Total	35					Total			Total	35				

Fig. 31 – ANOVA analysis used on peak penetration forces. Varied by α and θ .

Forward	Alpha 0	Alpha 15	Alpha 30	Alpha 45	ANOVA: Two-Factor With Replication	Alpha 0.05	Alpha 15	Alpha 30	Alpha 45	Total	ANOVA: Two-Factor With Replication	Alpha 0.01	Alpha 15	Alpha 30	Alpha 45	Total		
Theta 70	5.420743	4.6662	4.857869	7.681812	SUMMARY	Alpha 0	Alpha 15	Alpha 30	Alpha 45	Total	SUMMARY	Alpha 0	Alpha 15	Alpha 30	Alpha 45	Total		
	5.132728	4.86925	6.30598	8.00316														
	4.113866	6.284463	6.04475	7.097565														
Theta 45	9.08445	8.891883	6.987566	6.896255	Count	3	3	3	3	12	Count	3	3	3	3	12		
	7.792211	4.173249	7.168833	6.980475	Sum	14.66734	15.81991	17.2086	22.78254	70.47839	Sum	14.66734	15.81991	17.2086	22.78254	70.47839		
	6.255818	5.387816	8.813278	5.992637	Average	4.889112	5.273304	5.7362	7.594179	5.873199	Average	4.889112	5.273304	5.7362	7.594179	5.873199		
Theta 20	9.177357	8.137947	9.582961	9.880551	Variance	0.471493	0.777138	0.595659	0.210785	1.548788	Variance	0.471493	0.777138	0.595659	0.210785	1.548788		
	7.354217	8.054458	8.878774	10.82														
	7.532431	7.832034	6.816036	8.154929	Count	3	3	3	3	12	Count	3	3	3	3	12		
					Sum	23.13248	18.45295	22.96968	19.86937	84.42447	Sum	23.13248	18.45295	22.96968	19.86937	84.42447		
					Average	7.710826	6.150983	7.656559	6.623122	7.035373	Average	7.710826	6.150983	7.656559	6.623122	7.035373		
					Variance	2.005257	6.003194	1.011714	0.299907	2.183887	Variance	2.005257	6.003194	1.011714	0.299907	2.183887		
					Count	3	3	3	3	12	Count	3	3	3	3	12		
					Sum	24.064	24.02444	25.27777	28.85548	102.2217	Sum	24.064	24.02444	25.27777	28.85548	102.2217		
					Average	8.021335	8.008146	8.425924	9.618492	8.518474	Average	8.021335	8.008146	8.425924	9.618492	8.518474		
					Variance	1.01023	0.025004	2.067774	1.827153	1.367171	Variance	1.01023	0.025004	2.067774	1.827153	1.367171		
					Count	9	9	9	9	36	Count	9	9	9	9	36		
					Sum	61.86382	58.2973	65.45605	71.50738	253.66737	Sum	61.86382	58.2973	65.45605	71.50738	253.66737		
					Average	6.873758	6.477478	7.272894	7.945264	6.793833	Average	6.873758	6.477478	7.272894	7.945264	6.793833		
					Variance	3.105408	3.163676	2.358077	2.33609	2.33609	Variance	3.105408	3.163676	2.358077	2.33609	2.33609		
					ANOVA						ANOVA							
					Source of Variation	SS	df	MS	F	P-value	F crit	Source of Variation	SS	df	MS	F	P-value	F crit
					Sample	42.19088	2	21.09544	15.52533	4.71E-05	3.402826	Sample	42.19088	2	21.09544	15.52533	4.71E-05	5.613591
					Columns	10.58319	3	3.52773	2.596256	0.075813	3.008787	Columns	10.58319	3	3.52773	2.596256	0.075813	4.718051
					Interaction	12.90451	6	2.150751	1.58286	0.195297	2.508189	Interaction	12.90451	6	2.150751	1.58286	0.195297	3.666717
					Within	32.61062	24	1.358776				Within	32.61062	24	1.358776			
					Total	98.2892	35					Total	98.2892	35				

Fig. 32 – ANOVA analysis used on forward movement forces. Varied by α and θ .

Backward	Alpha 0	Alpha 15	Alpha 30	Alpha 45	ANOVA: Two-Factor With Replication					ANOVA: Two-Factor With Replication						
Theta 70	-1.00285	-0.49096	-1.05239	0.42904	SUMMARY					SUMMARY						
	-0.30996	-0.80963	-0.64363	-0.08654	Theta 70					Theta 70						
	-0.22026	0.085838	-0.46204	1.324868	Count	Sum	Average	Variance	Count	Sum	Average	Variance	Count	Sum	Average	Variance
Theta 45	0.986645	0.69127	-0.46152	-0.79134	3	-1.53308	-1.21475	1.667369	3	-3.23853	-3.23853	0.26988	3	-1.53308	-1.21475	1.667369
	-0.11944	-0.89364	1.426046	-0.00572	3	-0.51103	-0.40492	0.55579	3	-2.6988	-2.6988	0.44203	3	-0.51103	-0.40492	0.55579
Theta 20	-0.32407	-0.29973	0.505064	-0.43005	3	0.183432	0.206017	0.091429	3	0.510069	0.44203	0.44203	3	0.183432	0.206017	0.091429
	-1.1516	-0.34597	-0.73069	-1.40168	Count	Sum	Average	Variance	Count	Sum	Average	Variance	Count	Sum	Average	Variance
	-1.81557	0.221563	0.29987	0.42095	3	0.543128	-0.50209	1.469595	3	-1.22711	0.283516	0.283516	3	0.543128	-0.50209	1.469595
	-0.64393	-0.56992	-0.94812	-0.68578	3	0.181043	-0.16736	0.489865	3	-0.40904	0.023626	0.023626	3	0.181043	-0.16736	0.489865
					3	0.497215	0.641123	0.890896	3	0.15463	0.524112	0.524112	3	0.497215	0.641123	0.890896
					Theta 20					Theta 20						
					Count	Sum	Average	Variance	Count	Sum	Average	Variance	Count	Sum	Average	Variance
					3	-3.61111	-0.69433	-1.37894	3	-1.66651	-7.35088	-2.45296	3	-3.61111	-0.69433	-1.37894
					3	-1.2037	-0.23144	-0.45965	3	-0.5555	-0.61257	0.61257	3	-1.2037	-0.23144	-0.45965
					3	0.345219	0.166449	0.444467	3	0.843223	0.469339	0.469339	3	0.345219	0.166449	0.444467
					Total					Total						
					Count	Sum	Average	Variance	Count	Sum	Average	Variance	Count	Sum	Average	Variance
					9	-4.60106	-2.41117	-2.06741	9	-1.22626	-1.3625	0.650395	9	-4.60106	-2.41117	-2.06741
					9	-0.51123	-0.26791	-0.22971	9	-0.13625	0.616001	0.264726	9	-0.51123	-0.26791	-0.22971
					9	0.616001	0.264726	0.660602	9	0.650395	0.616001	0.264726	9	0.616001	0.264726	0.660602
					ANOVA					ANOVA						
					Source of Variation					Source of Variation						
					SS	df	MS	F	P-value	Fcrit	SS	df	MS	F	P-value	Fcrit
					2.433341	2	1.21667	2.935173	0.072386	3.402826	2.433341	2	1.21667	2.935173	0.072386	5.613591
					0.689835	3	0.229945	0.554734	0.649949	3.008787	0.689835	3	0.229945	0.554734	0.649949	4.718051
					5.152114	6	0.858686	2.071548	0.09476	2.508189	5.152114	6	0.858686	2.071548	0.09476	3.666717
					9.948336	24	0.414514				9.948336	24	0.414514			
					18.22363	35					18.22363	35				
					Total						Total					

Fig. 34 – ANOVA analysis used on backward movement forces. Varied by α and θ .

APPENDIX E

COMPLETE RAW DATA GRAPHS

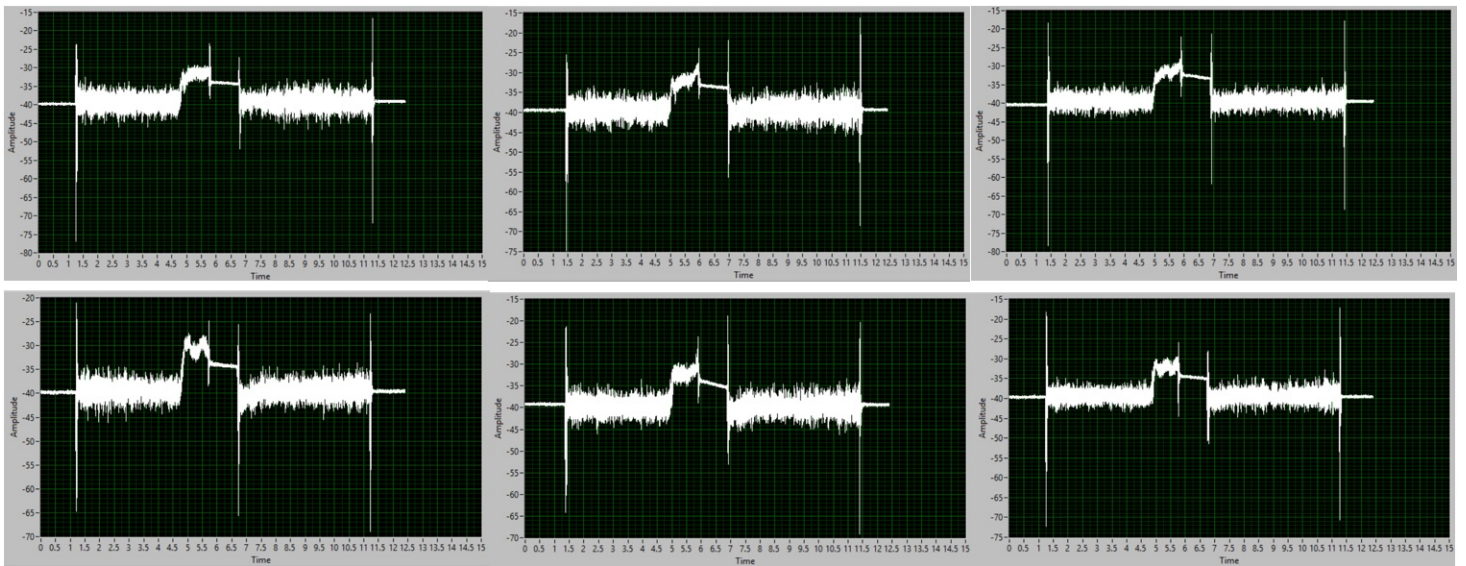


Fig. 35 – Force to time data graphs for clot sample. Taken from VI. 3 trials per row. Top is (0,0), bottom is (0,20).

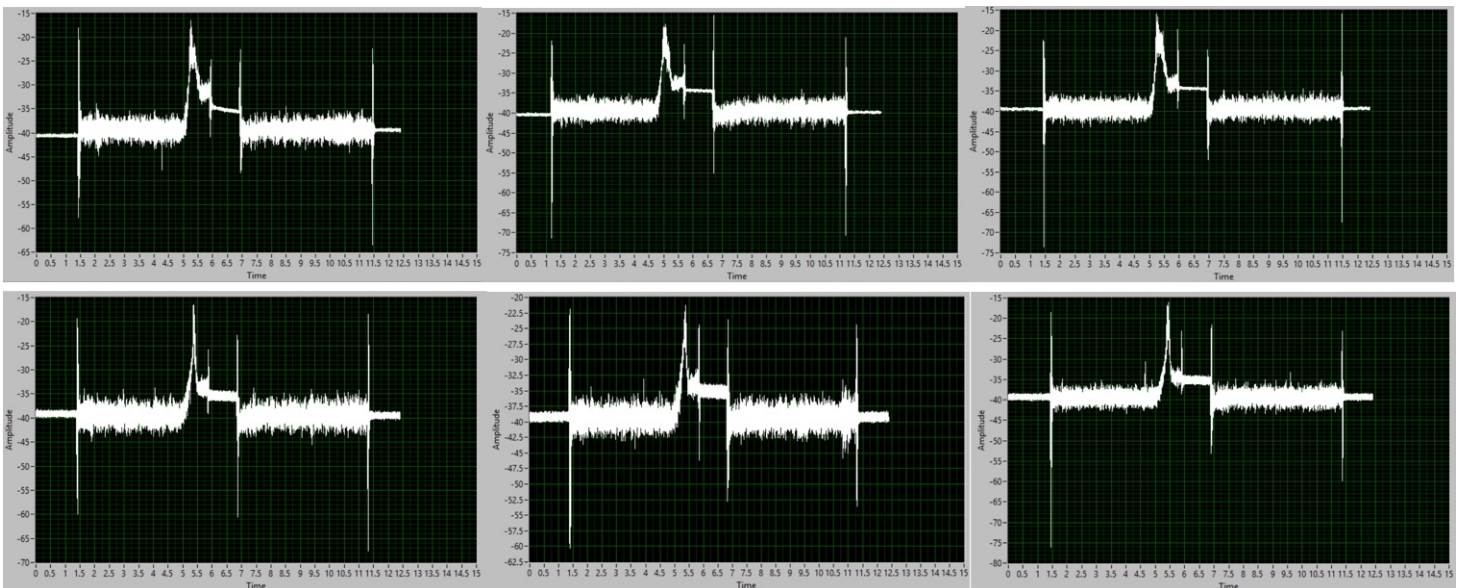


Fig. 36 – Force to time data graphs for clot sample. Taken from VI. 3 trials per row. Top is (0,45), bottom is (0,70).

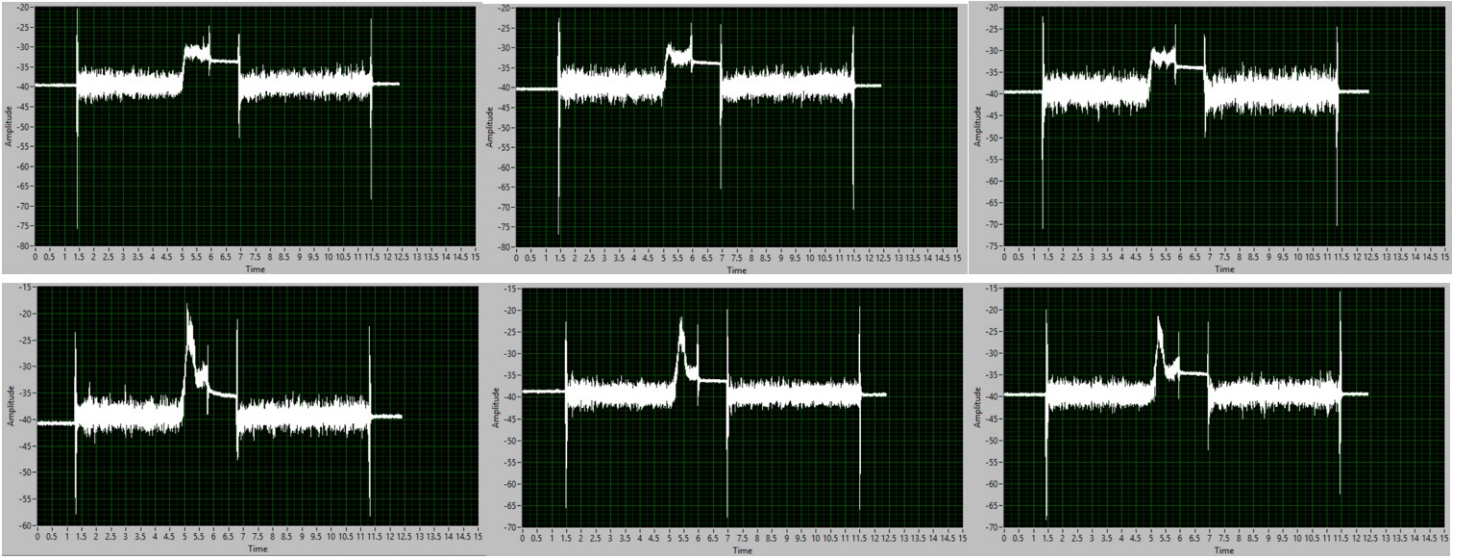


Fig. 37 – Force to time data graphs for clot sample. Taken from VI. 3 trials per row. Top is (15,20), bottom is (15,45).

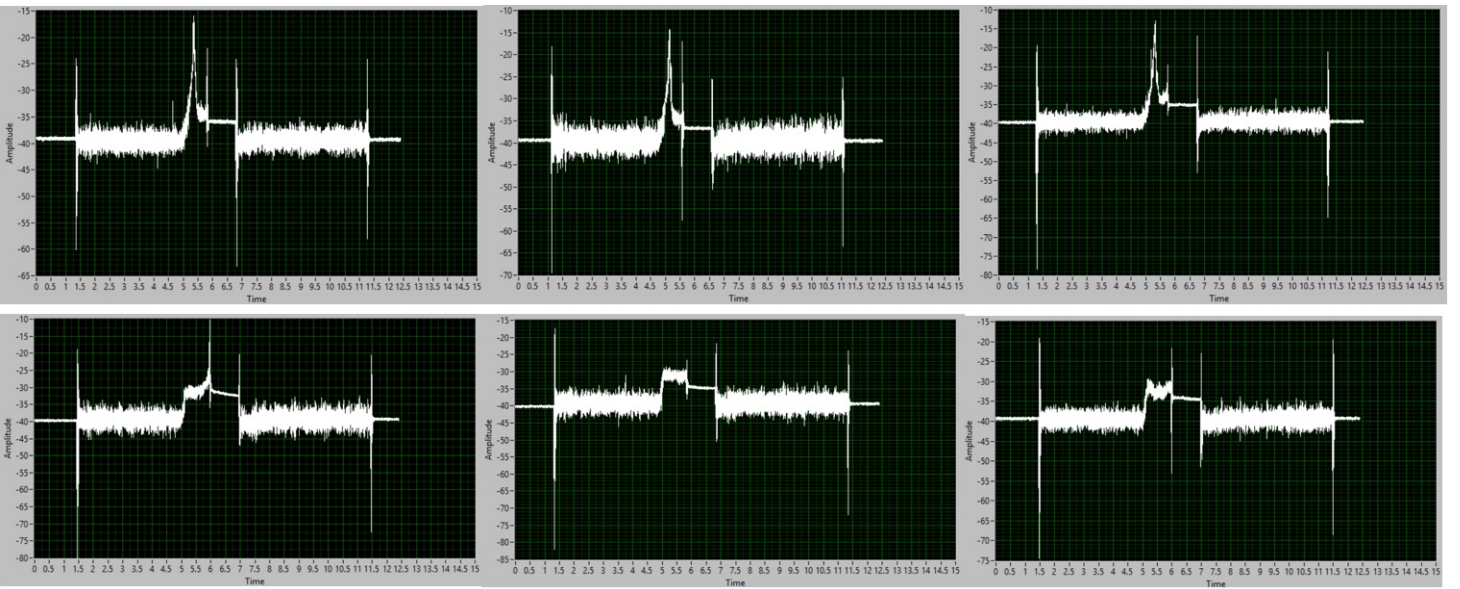


Fig. 38 – Force to time data graphs for clot sample. Taken from VI. 3 trials per row. Top is (15,70), bottom is (30,20).

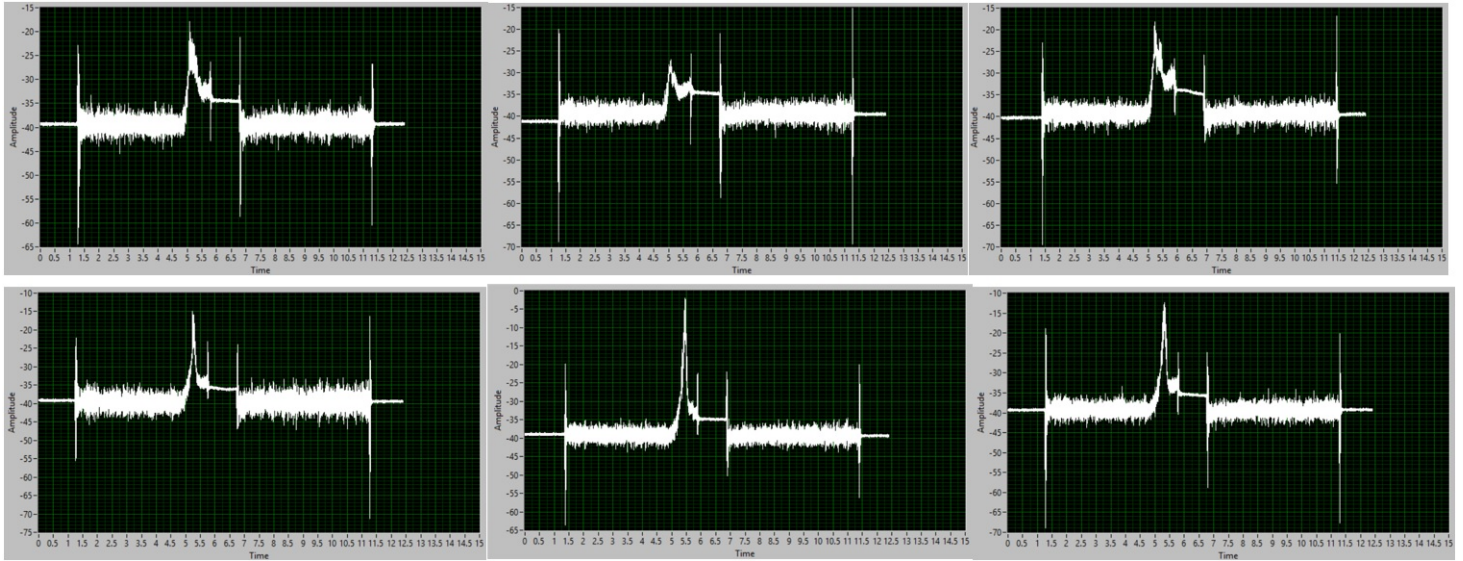


Fig. 39 – Force to time data graphs for clot sample. Taken from VI. 3 trials per row. Top is (30,45), bottom is (30,70).

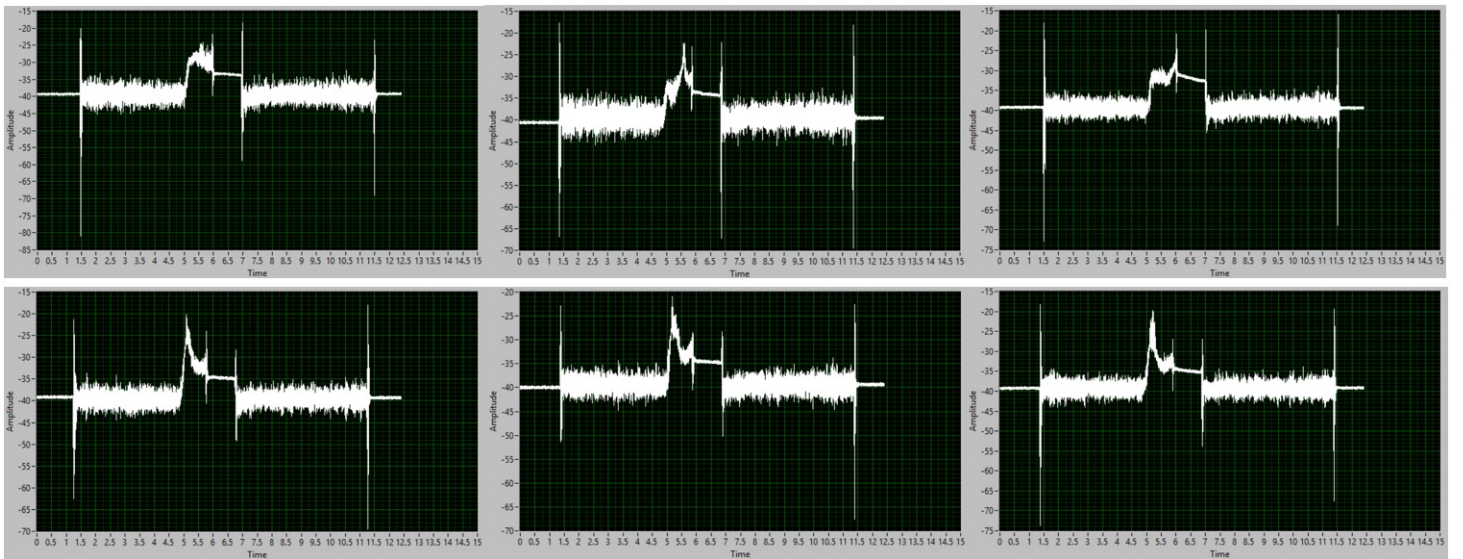


Fig. 40 – Force to time data graphs for clot sample. Taken from VI. 3 trials per row. Top is (45,20), bottom is (45,45).

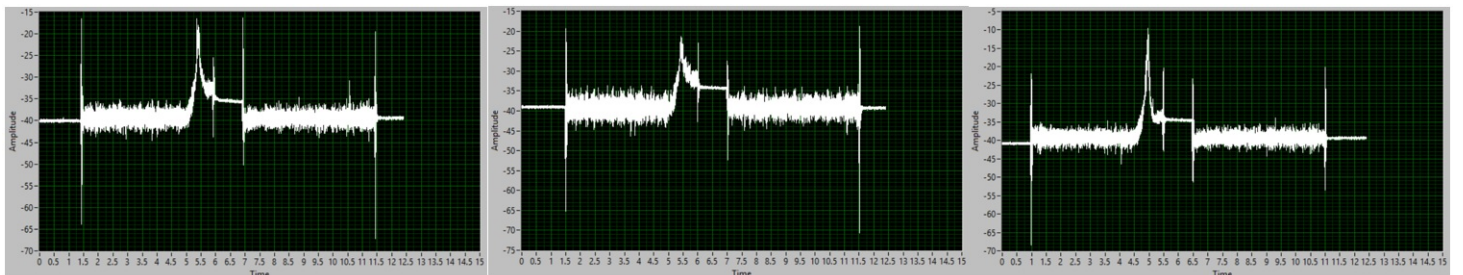


Fig. 41 – Force to time data graphs for clot sample. Taken from VI. 3 trials per row. Row is (45,70).

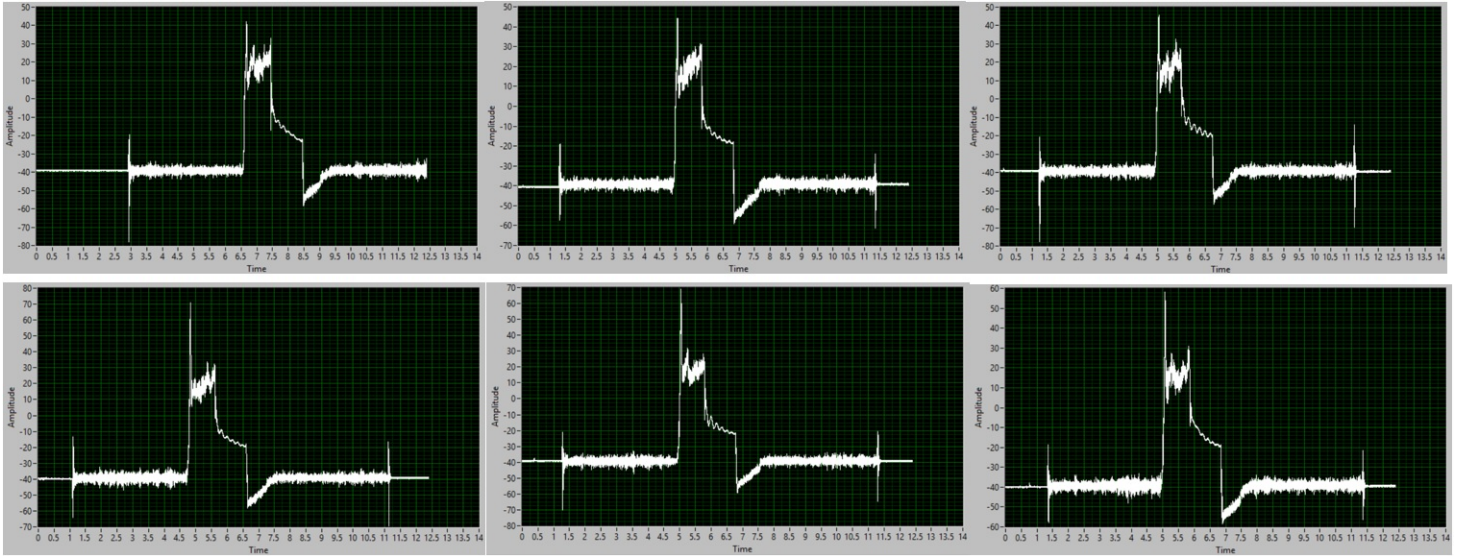


Fig. 42 – Force to time data graphs for agar sample. Taken from VI. 3 trials per row. Top is (0,0), bottom is (0,20).

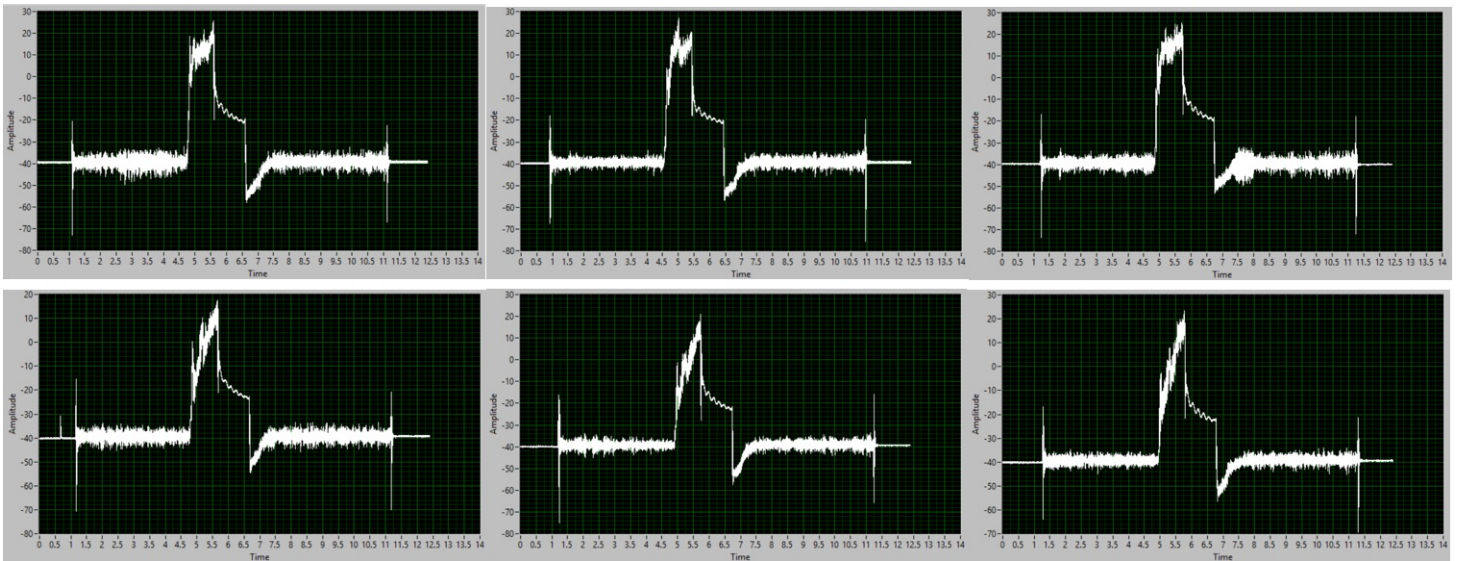


Fig. 43 – Force to time data graphs for agar sample. Taken from VI. 3 trials per row. Top is (0,45), bottom is (0,70).